Pergamon

Geochimica et Cosmochimica Acta, Vol. 58, No. 17, pp. 3595–3612, 1994

0016-7037/94 $6.00 + .00

0016-7037(94)00156-1

Diffusion and reaction in rock matrix bordering a hyperalkaline fluid-filled fracture

CARL I. STEEFEL* and PETER C. LICHTNER†
Mineralogisch-Petrographisches Institut, Universität Bern, Bern, Switzerland

(*Received May* 13, 1993; *accepted in revised form February* 14, 1994)

Abstract—Multicomponent diffusive and advective-dominant transport-reaction calculations are used to analyze water-rock alteration in rock matrix adjacent to a hyperalkaline fluid-filled fracture. The calculations indicate that rock alteration resulting from diffusive transport may be fundamentally different from that observed in the case of advective-dominant transport. Since advective-dominant and diffusive transport can result in differing reaction products as a function of time and space, the two transport processes may modify the chemical and physical properties of the rock at different rates.

We apply reactive transport calculations to an analogue of the Cretaceous and Tertiary marls proposed as host rocks for the Swiss low-level nuclear waste repository. Diffusion-reaction calculations predict that the rock matrix bordering high-pH fluid-filled fractures could be completely cemented within 10 to 500 years. The bulk of the porosity reduction occurs because of the precipitation of calcite resulting from the interdiffusion of Ca^{2+} and CO_3^{2-}. In contrast, advective-dominant transport results in the precipitation of calcite only as a replacement of dolomite. Both advective-dominated and diffusive transport result in a porosity increase within millimeters or less of the fracture wall, an effect which could widen the fracture and thus increase the rate of radionuclide transport along the fracture. Because solute diffusion is coupled to porosity and tortuosity change in the rock matrix, cementation causes the fracture to become physically and chemically isolated from the rock matrix if no expansion of the rock occurs. As a consequence, reaction-induced porosity reduction may potentially decrease the buffering and sorbing capacity of a fractured host rock, thus reducing the physical and chemical retardation of contaminants migrating along fractures. These effects may occur within the time required for radionuclides in the repository to decay to environmentally safe levels.

INTRODUCTION

A NUMBER OF STUDIES have presented quantitative models for coupled multicomponent chemical reactions and solute transport (e.g., KORZHINSKII, 1970; FRANTZ and MAO, 1976, 1979; WEARE et al., 1976; WALSH et al., 1984; LASAGA, 1984; LICHTNER, 1985, 1988, 1992; LICHTNER et al., 1986; BRYANT et al., 1987; SCHECHTER et al., 1987; KIRKNER and REEVES, 1988; LIU and NARASIMHAN, 1989a,b; NOVAK et al., 1989; STEEFEL and VAN CAPPELLEN, 1990; STEEFEL and LASAGA, 1992, 1994; YEH and TRIPATHI, 1991; BALASHOV and LEBEDEVA, 1991; BOUDREAU and CANFIELD, 1993; GUY, 1993; SEVOUGIAN et al., 1993). An important question with regard to reactive transport processes which has been largely neglected, however, is how water-rock reactions may differ in the case of diffusive vs. advective or advective-dominant transport. Aside from the differences in length scales which may occur, do the distributions of reaction products in space show similar patterns? Do completely different mineral assemblages form in the two cases? Do the chemical and physical properties of the rock change at different rates for the two modes of transport? The problem of diffusive transport and reactions is a very general one in the earth sciences. For example, coupled diffusion and reaction in fractured rock is a subject of longstanding interest to economic geologists studying hydrothermal vein formation. How economic mineralization in veins or fractures relates to "wall-rock alteration" has been studied for many years, although not with methods which explicitly and quantitatively couple diffusive transport to chemical reactions (e.g., SALES and MEYER, 1948, 1949, 1950; MEYER and HEMLEY, 1967; MEYER et al., 1968; BRIMHALL, 1977). "Diffusion metasomatism" has also been widely discussed in metamorphic geology (e.g., KORZHINSKII, 1970), although without considering the actual timescales for the processes involved.

Reactive transport modeling may be useful in performance assessment analyses of nuclear waste repositories where it is necessary to predict the evolution of the porosity, permeability, and tortuosity of the rock over geological periods of time. A great deal of research is in progress to assess the feasibility of placing nuclear waste in man-made repositories sited within natural rock formations. The host rock surrounding the repository is intended to act as a natural barrier to retard the migration of radionuclides away from the repository. The physical and chemical properties of the host rock, however, may not remain constant over the time required for the radionuclides to decay to safe levels. For example, chemical reactions can significantly modify the physical and chemical characteristics of the repository host rock. A number of possible effects can be cited: chemical reactions may (1) alter the local fluid flow regime by changing the permeability of the host rock (e.g., LICHTNER, 1985; ORTOLEVA et al., 1987; SANFORD and KONIKOW, 1989; STEEFEL and LASAGA, 1990; STEEFEL and LASAGA, 1994), (2) cause a change in the effective diffusion coefficient for ions in the

* *Present address:* Battelle, Pacific Northwest Laboratories, Interfacial Geochemistry Group, M.S. K3-61, P.O. Box 999, Richland, WA 99352, USA.
† *Present address:* Southwest Research Institute, Center for Nuclear Regulatory Analyses, 6220 Culebra Road, San Antonio, TX 78238-5166, USA.

pore fluids by changing the porosity and tortuosity of the host rock, and (3) result in a change in the neutralization and sorption capacity of the rock by modifying its chemical composition. Any of these phenomena could have a significant impact on the migration behavior of radionuclides.

The materials used in constructing a nuclear waste repository may themselves have a significant influence on the local groundwater chemistry. Cement has been proposed as a construction material for low-level nuclear waste repositories in several countries, including Switzerland, Great Britain, Sweden, and the USA. A concern with the use of cement as a construction material is that groundwaters which react with it may attain pH values as high as 13, thus creating a hyperalkaline plume very far from equilibrium with respect to the repository host rock. The hyperalkaline plume may cause significant alteration of the physical and chemical properties of the rock.

In this paper we present a model for coupled chemical reaction and diffusive transport to analyze the effects of water-rock interaction in the vicinity of a cement-bearing nuclear waste repository. The host rock considered is similar to that proposed as repository site by the Swiss in Cretaceous and Tertiary marls. We focus on the portion of the flow system where high-pH fluids, having percolated through the cementitious repository, infiltrate the marl along discrete fractures. In this analysis, we neglect the processes like calcification which might take place in the cement itself. A more thorough description of the processes taking place in the host rock would require a "dual porosity" model where reaction and transport along the fracture are coupled to diffusion and reaction in the adjacent rock matrix. In this paper we restrict ourselves to one-dimensional transport perpendicular to the fracture (Fig. 1). The effects of diffusion and reaction in the rock matrix are contrasted with those obtained when advective transport dominates. The problem of pure advective infiltration of a hyperalkaline plume has been examined in detail by LICHTNER and EIKENBERG (1994). The calculations are used to predict both the rate and spatial distribution of reaction-induced porosity change in rock matrix bordering a fracture filled with a high-pH fluid. We examine the feedback between the chemical reactions and the rates of diffusive transport by including a phenomenological relationship between the porosity and the tortuosity of the rock matrix.

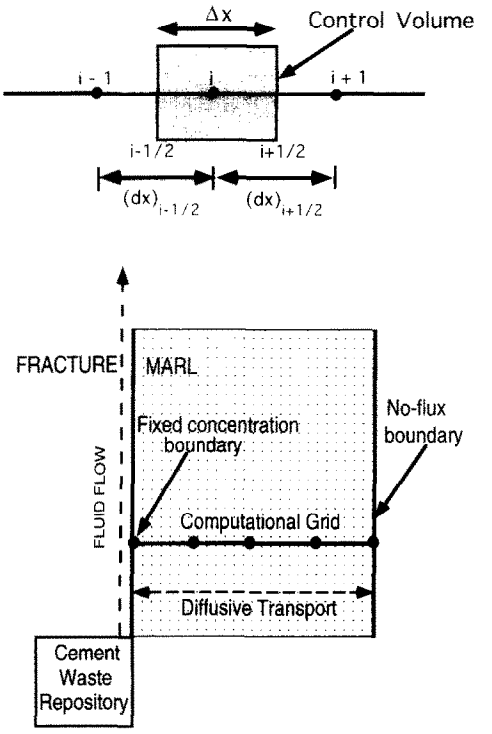

FIG. 1. Schematic representation of the physical setting of a fracture developed in a marl host rock and emanating from a cement-bearing nuclear waste repository. The calculations assume that flow in the fracture maintains a fluid composition along the fracture wall which is in equilibrium with cement. The lack of equilibrium between the minerals making up the marl and the high-pH fluid in the fracture generates diffusional fluxes between the two. The physical setting of the computational domain is shown along with the discretization scheme for a one-dimensional problem using integrated finite differences.

MATHEMATICAL FORMULATION OF THE MODEL

Conservation Equations

A continuum representation of coupled diffusive mass transport and chemical reactions can be described mathematically by a set of partial differential equations in time and space of the form

$$\frac{\partial}{\partial t}(\phi C_i) - \frac{\partial}{\partial x}\left(\phi D \frac{\partial C_i}{\partial x}\right) = R_i \quad (i = 1, 2, \ldots, N_{\text{tot}}), \qquad (1)$$

where C_i is the concentration of the ith species in solution (in units of mol m^{-3} solution), D is the coefficient for diffusion in porous media (m^2 s^{-1}), R_i (mol m^{-3} rock s^{-1}) is the net reaction rate of species i in solution, and N_{tot} is the total number of aqueous species. With the assumption of equilibrium among the various species in solution, it is possible to reduce the number of actual unknowns by partitioning the system between the primary or linearly independent species, C_j, and the secondary or linearly dependent species, X_i (REED, 1982; LICHTNER, 1985; KIRKNER and REEVES, 1988; YEH and TRIPATHI, 1989; STEEFEL and LASAGA, 1994). The concentrations of the secondary species can be written in terms of the concentrations of the primary species using the law of mass action for the equilibrium reactions which link them:

$$X_i = K_i^{-1} \gamma_i^{-1} \prod_{j=1}^{N_c} (\gamma_j C_j)^{\nu_{ij}} \quad (i = 1, \ldots, N_x), \qquad (2)$$

where the K_i are the equilibrium constants of the reaction written as the destruction of one mole of the secondary species. γ_i and γ_j are the activity coefficients for the secondary and primary species, respectively, ν_{ij} is the stoichiometric reaction coefficient, and N_c and N_x are the number of primary and secondary species in the system, respectively. If a "total" component concentration, Ψ_j, of the jth component is defined by

$$\Psi_j = C_j + \sum_{i=1}^{N_x} \nu_{ij} X_i, \qquad (3)$$

then the governing differential equations can be written in terms of the "total" concentrations (LICHTNER, 1985; KIRKNER and REEVES, 1988; YEH and TRIPATHI, 1989):

$$\frac{\partial}{\partial t}(\phi\Psi_j) - \frac{\partial}{\partial x}\left(\phi D \frac{\partial \Psi_j}{\partial x}\right) = R_j^{\min} \quad (j = 1, \ldots, N_c). \quad (4)$$

LICHTNER (1985) refers to Ψ_j as the "generalized concentration" because it may take on both negative and positive values. The reaction rates of the homogeneous (speciation) reactions in Eqn. 4 have been eliminated with Eqn. 3 (see LICHTNER, 1985; KIRKNER and REEVES, 1988), leaving only the mineral-fluid (heterogeneous) reactions, $R_j^{\min}$. In this work, all heterogeneous reactions are assumed to be irreversible. The heterogeneous reaction term $R_j^{\min}$ can be written as the sum of all the individual mineral-water reactions that affect the concentration of the jth species:

$$R_j^{\min} = -\sum_{m=1}^{N_m} \nu_{mj} r_m, \quad (5)$$

where r_m is the rate of precipitation or dissolution of mineral m per unit volume rock, ν_{mj} is the number of moles of j in mineral m (or stoichiometric coefficient if the reaction is written in terms of the dissolution of one mole of the mineral), and N_m is the number of minerals present in the rock. r_m is positive for precipitation and negative for dissolution.

Writing the conservation equations in terms of the total concentrations is only possible when the diffusion coefficients for all species are the same. Although this is in general not strictly true, particularly in the case of the H^+ ion (OELKERS and HELGESON, 1988), the assumption makes the solution of the reaction-transport equation simpler because the secondary species do not have to be individually transported. For a discussion of the case where the diffusion coefficients are not all the same, see LASAGA (1979) and LICHTNER (1985). We also assume that the diffusion coefficients do not depend on concentration, which is justified at the relatively low ionic strengths considered here (FELMY and WEARE, 1991).

The diffusion coefficient for porous media, D, can be expressed in terms of the diffusion coefficient in water, D_0, and a formation factor, F, according to

$$D = \frac{D_0}{\phi F}, \quad (6)$$

where F is defined as the ratio of the resistivity of the saturated porous medium over the resistivity of the pore solution alone (MARSILY, 1986). The factor, F, may be defined in numerous ways (see, for example, DULLIEN, 1979), but here a definition based on Archie's Law is used which gives the formation factor as

$$F = \phi^{-m}, \quad (7)$$

where m is the "cementation exponent" (DULLIEN, 1979). DULLIEN (1979) reports values of m which range between about 1.3 and 2.5.

Initial and Boundary Conditions

The solute concentration boundary conditions at the fracture inlet are given by

$$C_j(x = 0, t) = C_j^0(t), \quad (8)$$

or equivalently,

$$\Psi_j(x = 0, t) = \Psi_j^0(t), \quad (9)$$

where we have considered the possibility that the boundary conditions may depend on time. If the rock consists of a set of parallel fractures, then the symmetry plane halfway between two adjacent fractures corresponds to a no-flux condition given by

$$\frac{\partial \Psi_j}{\partial x} = 0. \quad (10)$$

The initial conditions for the solute concentrations and the mineral volume fractions, ϕ_m, are given by

$$C_j(x, t = 0) = C_j^{in} \quad (11)$$

and

$$\phi_m(x, t = 0) = \phi_m^{in}. \quad (12)$$

The initial solute concentrations are determined by some combination of either mineral equilibria, charge, or total concentration constraints.

Kinetic Formulation

We use a kinetic rate law based on the assumption that attachment and detachment of ions from mineral surfaces is the rate-limiting step (STEEFEL and LASAGA, 1994). The rate laws used for mineral precipitation and dissolution in 1DREACT (STEEFEL and LASAGA, 1994; see Appendix) are based loosely on transition state theory (e.g., LASAGA, 1981; AAGAARD and HELGESON, 1982; LASAGA, 1984). This formulation gives the dependence of the rate on the saturation state of the solution. The ion activity product, Q_m, is defined by

$$Q_m = \prod_{j=1}^{N_c} a_j^{\nu_{mj}}, \quad (13)$$

where the a_j are the activities of the primary species used in writing the dissolution reaction for the mineral, and the ν_{mj} are the stoichiometric coefficients for the reaction. This leads to the following form for the rate law of crystal growth and dissolution of a mineral (see LASAGA, 1981, 1984; AAGAARD and HELGESON, 1982; STEEFEL and VAN CAPPELLEN, 1990; STEEFEL and LASAGA, 1994)

$$r_m = \operatorname{sgn}\left(\log\left[\frac{Q_m}{K_m}\right]\right) A_m k_m \left(\prod_{i=1}^{N_c+N_x} a_i^{p}\right) \left|\left(\frac{Q_m}{K_m}\right)^{\mathcal{M}} - 1\right|^n, \quad (14)$$

where k_m is the growth or dissolution rate constant, a_i is the activity of an inhibiting or catalyzing species raised to an empirically determined power p, and $\mathcal{M}$ and n are two positive numbers which are also normally determined empirically. The vertical bars | | refer to the absolute value of the quantity and the term sgn (log $[Q_m/K_m]$) gives the sign of the expression, negative if the fluid is undersaturated and positive if the fluid is supersaturated with respect to the mineral. This formulation ensures that the reaction rate, r_m, has the correct sign when $n \neq 1$. This is in contrast to the expression given in STEEFEL and VAN CAPPELLEN (1990) (as pointed out by MERINO et al., 1993), although the correct expression was

used in the calculations presented in that work. We have not explicitly included a pH dependence to the reaction rate in the calculations presented here, although the reaction rate constants used in the calculations are characteristic of high-pH conditions. Equation 1 is solved numerically using the code 1DREACT which is discussed in the Appendix and in STEEFEL and LASAGA (1994).

Mineral Alteration

The mineral abundances as a function of time and space are given by

$$\frac{\partial \phi_m}{\partial t} = V_m r_m, \tag{15}$$

where V_m is the molar volume of mineral m, and ϕ_m is its volume fraction per unit volume rock. By computing the mineral volume fractions as a function of time, the porosity can be immediately calculated from the expression

$$\phi = 1 - \sum_{m=1}^{N_m} \phi_m. \tag{16}$$

This assumes that there are no other effects on the porosity like compaction or dilation.

VERIFICATION OF THE ALGORITHM

The algorithm can be verified in part by comparing the results of the numerical calculations using the code 1DREACT with the semi-analytical results given by LICHTNER (1991) for a three-component system characterized by local equilibrium, equal diffusion coefficients for all species, purely diffusive transport, constant porosity, and concentration boundary conditions. LICHTNER (1991) analyzed a hypothetical system containing the solutes A, B, and C which are allowed to form two distinct minerals: AB_s, which initially makes up the rock, and AC_s, which replaces AB_s. The inlet solution at the boundary, $x = 0$, is undersaturated with respect to both minerals. The hypothetical system can be taken to represent the replacement of gypsum by calcite if the pH is assumed to be constant and the solute species A, B, and C correspond to Ca^{+2}, SO_4^{2-}, and HCO_3^-, respectively. Although the analytical solution yields the position of the mineral AB_s (gypsum) as a function of time, the internal precipitation rate within the AC_s zone (calcite) must be determined numerically (LICHTNER, 1991). Fortunately, the integration is straightforward and introduces a minimal error, so that the result can be taken as nearly exact. Since the method used by LICHTNER (1991) is fundamentally different from the one used in this paper, a comparison between the two approaches is useful in any case.

The code 1DREACT has no provision currently for the assumption of local equilibrium between the fluid and the minerals, but a reasonably close approximation can be obtained by using sufficiently large reaction rate constants. The numerical calculation was carried out using the same boundary conditions, equilibrium constants, diffusion coefficient, and initial volume fractions as in the pure diffusion problem considered by LICHTNER (1991). A reaction rate of 10^{-3} mol m^{-2} s^{-1} and a surface area of 500 m^2 was used for both minerals AB_s and AC_s.

The reaction rate of mineral AC_s after 100 years is shown in Fig. 2a,b. Between $x = 0$ and about 0.92 cm, both minerals AB_s and AC_s have disappeared from the rock since the fluid is undersaturated with respect to them at $x = 0$, and the rate vanishes. The position of the dissolution front of the mineral AC_s occurs at about 0.92 cm and marks the start of the zone AC_s while the precipitation peak at about 2.35 cm marks the position of the front where mineral AC_s is replacing mineral AB_s. The peaks in the rate, marking the positions of the two reaction fronts, represent the kinetic expression of what in the local equilibrium limit is a delta function. Figure 2b is a magnification of the reaction rates in Fig. 2a in order to show more clearly the internal precipitation rate of mineral AC_s. The broken line represents the rate obtained numerically from the code 1DREACT and is compared with the (semi-analytical) local equilibrium results (solid line) obtained by LICHTNER (1991). Bordering the internal precipitation zone in the kinetic (numerical) case are the (truncated) dissolution and precipitation peaks corresponding to the position of the reaction fronts. These peaks are not shown in the local equilibrium case where they would appear as delta functions due to the jump discontinuity in the solute concentrations across the reaction fronts. 1DREACT slightly overestimates the magnitude of the internal precipitation rate over the first part of zone AC. In addition, the beginning and end of the internal AC_s precipitation zone in the numerical calculation lag about 0.5 mm behind the positions in the local equilibrium case. Despite these discrepancies, the agreement between the two is good and it indicates that the numerical methods employed in 1DREACT can be used to track reaction fronts in the multicomponent case. A complete validation of the numerical model would require a more thorough error analysis of the effects of different grid spacings and time steps.

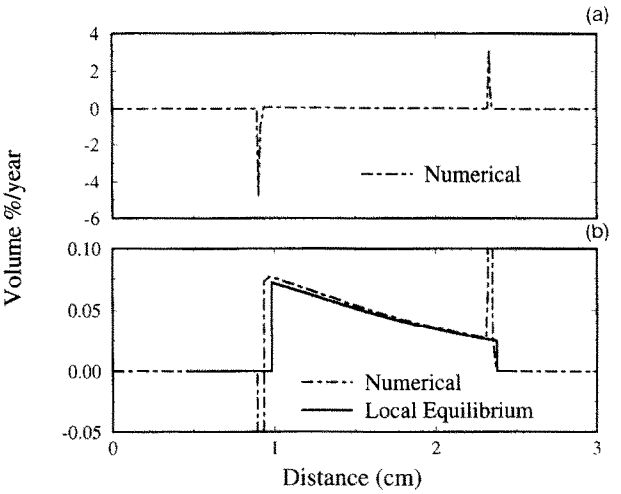

FIG. 2. (a) Reaction rate for mineral AC_s at 100 years from the numerical code 1DREACT. The sharp dissolution and precipitation peaks correspond to the positions of the reaction fronts. (b) Comparison of internal precipitation rates of mineral AC_s obtained from a semi-analytical, local equilibrium calculation (LICHTNER, 1991) and numerically by the code 1DREACT.

APPLICATION TO THE PROPOSED SWISS LOW-LEVEL REPOSITORY SITE

The remainder of the paper is devoted to an analysis of some of the chemical and physical effects of solute diffusion from a hyperalkaline fluid-filled fracture into a marl rock matrix. The use of a fluid composition saturated with respect to portland cement as a fixed boundary condition along the fracture wall implies that the fluid in the fracture has not been affected by reaction with the marl host rock. Physically, this would be the case where the flow velocity in the fracture was infinite (or more practically, very large), or to the region close to the fracture inlet. In order to consider the effects of a partly reacted fluid in the fracture, a dual porosity model is necessary.

The calculations are carried out with and without coupling the change in porosity (and thus, the diffusivity) caused by mineral reactions. The rock matrix is assumed to be immobile. In this case, if the porosity is updated it must tend towards zero as cementation proceeds. In a natural setting the rock matrix could expand, thus allowing precipitation to continue for extended periods of time without reducing the porosity. Although this second alternative is not explicitly modeled because of the assumption that the rock matrix is immobile, the "constant porosity" assumption can be used to obtain an approximate representation of the solute concentration profiles in this case. The "constant porosity" approximation is the endmember case in which the effective diffusion coefficient in the rock remains constant.

Cement and Marl Geochemistry

Geochemistry of the cement

Cement-based materials are used or have been proposed for use in the containment of contaminants in a large number of environments (REARDON, 1992). The chemistry of portlandite-based cement, however, is complicated and much work remains to be done even to establish its thermodynamic properties. The problem is further complicated by the fact that the dissolution of cement is incongruent (BERNER, 1992; REARDON, 1992). The composition of fluids emanating from a cement-bearing repository, therefore, may change over time.

A summary of the thermodynamic properties of cement is provided by LEA (1970). Hydrated cements contain a number of compositionally complex phases with variable thermodynamic properties. In addition, at the low temperatures prevailing in the vicinity of a low-level repository, many of the secondary phases are crypto-crystalline, making their identification and thermodynamic characterization more difficult. Despite these difficulties, a simplified phase composition which is compatible with analytical porewater data (KALOUSEK, 1952; GREENBERG and PRICE, 1957; GREENBERG and CHANG, 1965; ATKINSON et al., 1987) can be assumed on the basis of hydration models (GLASSER et al., 1988; BERNER, 1987).

The two most important phases in the hydration of a Ca-rich cement are portlandite ($Ca(OH)_2$) and various calcium silicate hydrates (referred to as CSH-gels). The presence of these two phases leads to porewater compositions with high OH^- and low silica activities (ATKINS and GLASSER, 1992; BERNER, 1992; REARDON, 1992; LICHTNER and EIKENBERG, 1994). While the activity of silica in the SiO_2-H_2O system increases with increasing pH (BUSEY and MESMER, 1977; THORNTON and RADKE, 1933; EIKENBERG, 1990; LICHTNER and EIKENBERG, 1994), in the CaO-SiO_2-H_2O system, the activity of silica actually decreases above about pH = 10 due to the precipitation of the CSH-gels (GREENBERG and CHANG, 1965; SARKAR et al., 1982; LICHTNER and EIKENBERG, 1994). As a result, the dissolution of silica-bearing phases (like quartz, muscovite, chlorite, and clays) at high pH can cause (1) an increase in porosity at the cement-marl contact as silicate minerals dissolve, as well as (2) a decrease in porosity because of the precipitation of large quantities of CSH-gels further from the contact in the marl. Significant porosity reduction can result from the precipitation of CSH$^-$ phases. Secondary amorphous and cryptocrystalline CSH-phases such as okenite, foshagite, tobermorite, and hillebrandite, in addition to zeolites and authigenic feldspars, have formed in a natural analogue of a cementitious system in northern Jordan (KHOURY and NASSIR, 1982).

Cement porewater compositions

As pointed out above, the dissolution of portlandite-based cement occurs incongruently, with preferential early release of highly soluble NaOH and KOH, followed later by calcium hydroxide. The high NaOH and KOH concentrations can lead to cement porewater pH values above 13. The transient degradation of the cement is generally attributed to the slow diffusion of elements from the cores of unreacted alkali-rich cement minerals (BERNER, 1990, 1992; REARDON, 1992; ATKINS and GLASSER, 1992). The alkalies are present in cement in the form of solid solutions with readily-soluble sulfates and as minor constituents with clinker phases alite, belite, aluminate, and ferrite. Thus, the system is not in equilibrium and solubility constraints do not apply for K and Na. Since Na and K typically make up less than 5% of cement, they should be leached gradually from the cement, leading eventually to porewater compositions dominated by Ca^{2+} with pH values between 12 and 13 (BERNER, 1992). Little is known, however, about the actual time dependence of cement degradation. BERNER (1992) calculated the evolution of the cement pore compositions by assuming that within each water-exchange cycle, 5% of the remaining Na and K were leached from the cement. He predicted that Ca would dominate the porewater chemistry after about 100 cycles. To relate these water-exchange cycles to real time requires a knowledge of the local fluid flux through the cement. BERNER (1992) estimated that each cycle would last 1 to 100 years, suggesting that the Na- and K-rich stage could last from 100 to 10,000 years. At present it is not possible to predict with certainty the partitioning of alkalies between solid and liquid phases.

In this paper, we address the problem of the incongruent dissolution of cement by considering three different scenarios. Most of the calculations are carried out with a cement porewater composition which has low Na and K concentrations

which are determined by the ambient marl groundwater and which has a solution pH of 12.54. In order to compare the behavior of the Ca-rich system with that of a Na- and K-rich system, we also carry out calculations using higher Na + K concentrations and higher pH values. We compare calculations in which the solution is assumed to remain constant at a total Na + K concentration = 0.3 M and a pH = 13.25 with calculations in which the Na and K gradually decrease with time over 1,000 years. The concentrations of species in the cement porewater are determined by a number of constraints. Some are fixed by equilibrium constraints between the pore fluid and the minerals typically found in the cement (portlandite, ettringite, calcite, katoite, brucite, foshagite). Others are either from the local groundwater or they are assumed to result from the degradation of the cement (e.g., Na and K). The pH is obtained by charge balance. The composition of the Ca-rich cement porewater is given in Table 1 and the composition of the Na + K-rich cement porewater is given in Table 6. The cement porewaters serve as the boundary condition at $x = 0$ for the diffusion-reaction calculations.

Marl composition

The Cretaceous and Tertiary marls in the vicinity of the proposed Swiss low-level nuclear waste repository site display variable modal compositions (LICHTNER and EIKENBERG, 1994). The marls consist primarily of calcite, dolomite, muscovite, quartz, chlorite, and pyrite (LICHTNER and EIKENBERG, 1994). A slightly idealized modal composition without pyrite and with kaolinite substituted for chlorite was used in the calculations (Table 2). Mercury injection measurements on the marl indicate a porosity of about 2% (M. Mazurek, pers. commun., 1992).

Marl porewater compositions

The groundwaters at the Wellenberg site show two distinct chemical compositions, a NaCl-type with an ionic strength $\approx$0.1 M and a $NaHCO_3$-type water with an ionic strength $\approx$0.02 M (J. Pöttinger, pers. commun.; LICHTNER and EIKENBERG, 1994). The $NaHCO_3$-type water was used to specify the initial composition of the marl groundwater in this study (Table 3).

Table 1. Solute concentrations and constraints for the low Na-K cement pore water used as a boundary condition in the calculations.

	Concentration (mol/l)	Constraint
OH^-	3.61×10^{-2}	charge balance
$Al(OH)_4^-$	1.53×10^{-5}	katoite
K_{tot}	1.02×10^{-4}	marl groundwater
Na_{tot}	1.83×10^{-2}	marl groundwater
Ca^{2+}	8.53×10^{-3}	portlandite
Mg^{2+}	4.43×10^{-9}	brucite
$SiO_{2(aq)}$	8.44×10^{-10}	foshagite
CO_3^{2-}	1.64×10^{-6}	calcite
SO_4^{2-}	5.58×10^{-5}	ettringite
Cl_{tot}	1.03×10^{-3}	marl groundwater
T(°C)	25	
I(M)	4.59×10^{-2}	
pH	12.46	

Table 2. Initial modal composition of the Wellenberg marl used in the calculations in this study. Assumes an initial porosity of 2%.

Mineral	Volume %
calcite	45
dolomite	5
muscovite	20
quartz	15
kaolinite	13

Calculation Parameters

The reaction rate constants used in all of the calculations are given in Table 4. Although the calculations do not include an explicit pH dependence to the rates (see Eqn. A3), the rate constants used for muscovite, kaolinite, K-feldspar, quartz, and albite were determined under high pH rather than neutral conditions (BRADY and WALTHER, 1989). Equilibrium constants for minerals and aqueous complexes reactions are given in Tables 4 and 5, respectively. All minerals are treated as pure phases. Activity coefficients are calculated with an extended Debye-Hückel formulation. All the calculations without a porosity feedback used a value of 1.5 for the cementation exponent in Archie's Law, giving an effective diffusion coefficient, D, of 1.4×10^{-6} cm^2 s^{-1}. In the calculations with a porosity feedback, cementation exponents of 1.25, 1.5, and 2.0 were compared.

A total of 200 to 300 grid points were used to discretize the spatial domain. In most cases, a grid spacing of 0.5 mm was used between $x = 0$ (the fracture wall) and 5 cm from the fracture wall, a spacing of 3 mm between 5 and 20 cm, and a spacing of 6 mm between 20 and 50 cm. The time steps used in the calculations were allowed to vary with time, beginning with less than a second and increasing up to a maximum value of 1 year.

Calculations with Constant Porosity

The evolution of the solution pH up to 30 years is plotted against distance (in cm) from the fracture wall in Fig. 3. The

Table 3. Solute concentrations and constraints for the marl pore water used as an initial condition in the calculations.

	Concentration (mol/l)	Constraint
OH^-	2.30×10^{-6}	
$Al(OH)_4^-$	2.20×10^{-8}	muscovite
K_{tot}	5.11×10^{-5}	
Na_{tot}	1.79×10^{-2}	
Ca^{2+}	3.93×10^{-5}	calcite
Mg^{2+}	2.49×10^{-6}	dolomite
$SiO_{2(aq)}$	1.67×10^{-4}	chalcedony
CO_3^{2-}	2.32×10^{-2}	
SO_4^{2-}	1.15×10^{-4}	
Cl^-	1.66×10^{-6}	charge balance
T(°C)	25	
I(M)	1.81×10^{-2}	
pH	8.3	

Table 4. Reaction rate constants and equilibrium constants used in the calculations.

Mineral	$k_{25°C}$ (moles m^{-2} s^{-1})	Log K^1_{eq}	$\mathcal{M}$	n
Calcite	3×10^{-6}	-8.48	0.5	2
Dolomite	1×10^{-9}	-18.14	1	1
Muscovite	1×10^{-12}	-27.43	1	1
Quartz	1×10^{-11}	-4.00	1	1
Kaolinite	1×10^{-12}	-11.20	1	1
Albite	1×10^{-11}	-20.24	1	1
Chalcedony	1×10^{-11}	-3.73	1	1
K-feldspar	1×10^{-11}	-23.28	1	1
Gibbsite	1×10^{-10}	-1.36	1	1
Natrolite	1×10^{-10}	-27.48	1	1
Laumontite	1×10^{-10}	-32.34	1	1
Analcime	1×10^{-10}	-15.94	1	1
Sepiolite	1×10^{-11}	-81.52	1	1
Brucite	1×10^{-9}	-11.69	1	1
Ettringite	1×10^{-9}	-43.94	1	1
Hillebrandite	1×10^{-9}	-19.68	1	1
Katoite	1×10^{-9}	-23.04	1	1
Foshagite	1×10^{-9}	-48.96	1	1
Tobermorite	1×10^{-9}	-70.95	1	1
Portlandite	1×10^{-9}	-5.44	1	1

1. All equilibrium constants from the EQ3/EQ6 database (Wolery et al., 1990) except for tobermorite, foshagite, and hillebrandite which are from Lichtner and Eikenberg (1994). All reactions written as the destruction of 1 mole of the mineral and using the primary species OH^-, $Al(OH)_4^-$, K^+, Na^+, Ca^{2+}, Mg^{2+}, $SiO_{2(aq)}$, CO_3^{2-}, SO_4^{2-}, Cl^-, and H_2O.

Table 5. Equilibrium constants for species in the calculations.

Species	Log K^1_{eq}
H^+	14.00
$Al(OH)^{2+}$	24.85
$Al(OH)_2^+$	15.94
$Al(OH)_{3(aq)}$	8.01
Al^{3+}	33.83
$H_2SiO_4^{2-}$	-5.08
$H_3SiO_4^-$	-4.18
HCO_3^-	3.67
$CO_{2(aq)}$	11.32
HSO_4^-	12.02
$H_2SO_{4(aq)}$	29.01
$NaHCO_{3(aq)}$	3.51
$NaCO_3^-$	-0.51
$NaOH_{(aq)}$	0.18
$NaSO_4^-$	-0.82
$NaH_3SiO_{4(aq)}$	-5.33
$MgCO_{3(aq)}$	-2.98
$MgH_2SiO_{4(aq)}$	-10.51
$MgH_3SiO_4^+$	-5.45
$MgHCO_3^+$	2.63
$MgOH^+$	-2.21
$MgSO_{4(aq)}$	-2.41
$MgCl^+$	0.13
$CaH_2SiO_{4(aq)}$	-9.43
$CaH_3SiO_4^+$	-5.20
$Ca(H_3SiO_4)_{2(aq)}$	-12.93
$CaHCO_3^+$	2.62
$CaOH^+$	-1.14
$CaSO_{4(aq)}$	-2.11
$KOH_{(aq)}$	0.46
KSO_4^-	-0.88

1. All equilibrium constants for species from the EQ3/EQ6 database. All reactions written as the destruction of 1 mole of the species and using the primary species OH^-, $Al(OH)_4^-$, K^+, Na^+, Ca^{2+}, Mg^{2+}, $SiO_{2(aq)}$, CO_3^{2-}, SO_4^{2-}, Cl^-, and H_2O.

effect of the diffusion of species into the marl rock matrix from the fracture can be seen out to 50 cm by 10 years. The solution pH quickly attains a steady state within 10 cm of the fracture wall. Note that a relatively large distance is required for the marl to neutralize the pH, despite the fact that the reaction rate constants used for the phases muscovite, kaolinite, albite, and K-feldspar are 100 times larger than

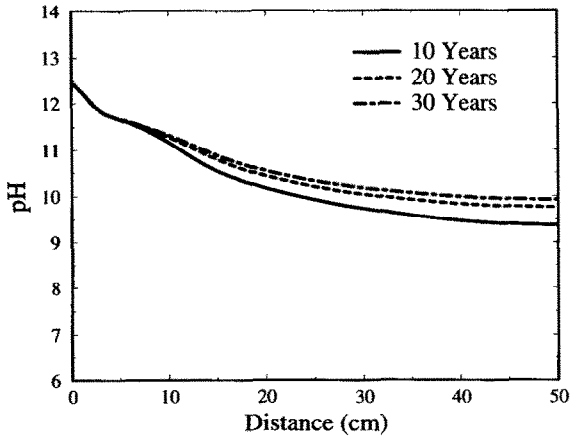

FIG. 3. Time evolution of pH in simulations assuming a constant porosity in the transport equations. The fracture wall, at $x = 0$, is in equilibrium with cement at a pH of 12.45. Boundary conditions for the calculation are given in Table 1 and the initial conditions are given in Table 3.

those measured at 25°C in the neutral pH range. The inflections in the pH profiles are the result of the precipitation and dissolution of various mineral phases. Figure 4a is a plot of the mineral reaction rates (in units of moles m^{-3} bulk rock yr^{-1}) at 50 years, with precipitation represented by positive values of the rate and dissolution indicated by negative values. For this choice of rate constants and surface areas, the minerals included in Fig. 4a are the most important phases within 5 cm of the fracture wall. Calcite begins to precipitate within a very short distance of the fracture wall, primarily due to the production of CO_3^{2-} resulting from the dissolution of dolomite. The precipitation of brucite accounts for most of the pH drop between 0.2 and 1.4 cm of the fracture according to

$$CaMg(CO_3)_2 + Ca^{2+} + 2\,OH^- \rightarrow 2\,CaCO_3 + Mg(OH)_2. \quad (17)$$

In this region, reaction 17 conserves both CO_3^{2-} and Mg^{2+}.

Between 1.4 and 1.75 cm from the fracture wall, a peak in the calcite precipitation rate occurs which is not balanced by the brucite and dolomite rates, indicating that reaction

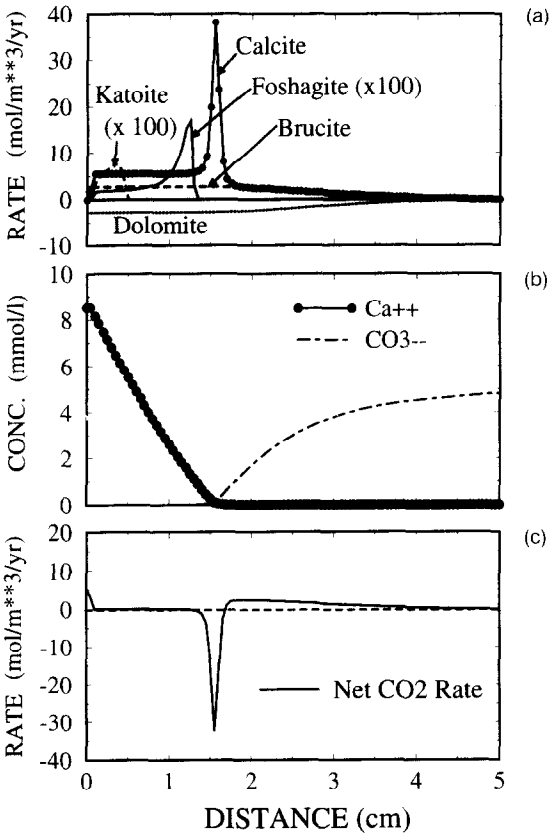

FIG. 4. (a) Reaction rates (mol m^{-3} $year^{-1}$) at 50 years for the minerals calcite, dolomite, brucite, foshagite, and katoite. The rates for foshagite and katoite are multiplied by 10 to make them visible. Calculations assume a constant porosity in the transport equations. Within about 1.3 cm of the fracture wall, the reaction conserves CO_3^{2-} and Mg. Between about 1.3 and 1.75 cm, however, CO_3^{2-} diffusing in from the marl to the right results in a precipitation peak in calcite which is not matched by peaks in brucite and dolomite. Filled circles on calcite precipitation rate indicate the actual discretization used in calculation. (b) Concentration profiles for Ca^{2+} and CO_3^{2-} (in mol/L solution). The interdiffusion of Ca^{2+} and CO_3^{2-} result in a calcite precipitation peak at about 1.5 cm from the fracture wall. Calculations assume a constant porosity in the transport equations. (c) Net reaction rate of total CO_2 plotted vs. distance from the fracture wall. Note that there is a net consumption of CO_2 at about 1.5 cm where the precipitation rate of calcite exceeds that of dolomite (Eqn. 18) and a net production of CO_2 between 1.75 and 4 cm from the fracture where the rate of dolomite dissolution equals the rate of calcite precipitation (Eqn. 20). Calculations assume a constant porosity in the transport equations.

17 no longer holds. The appropriate reaction at 1.55 cm from the fracture wall is instead

$$CaMg(CO_3)_2 + 11.8\ CO_3^{2-} + 12.8\ Ca^{2+} + 2\ OH^- \rightarrow 13.8\ CaCO_3 + Mg(OH)_2. \quad (18)$$

In this case, Ca^{2+} diffuses into the reaction zone from the fracture ($x = 0$ in Fig. 4) while the dominant carbonate species CO_3^{2-}, which is present only at very low concentrations in the fracture, diffuses into the zone from the marl to the right. This can be seen more clearly by plotting the concentration profiles of Ca^{2+} and CO_3^{2-} vs. distance from the fracture wall (Fig. 4b). Since concentration gradients create diffusive fluxes according to Fick's Law, the opposing slopes of the CO_3^{2-} and Ca^{2+} result in interdiffusion which in turn causes the precipitation of calcite. The dynamics is clarified further by examining a plot of the net rate of production or consumption of total CO_2 vs. distance from the fracture wall (Fig. 4c). The net rate, R_{CO_2}, is determined from Eqn. 5:

$$R_{CO_2} = -r_{calcite} - 2r_{dolomite}. \quad (19)$$

The calcite precipitation peak at about 1.55 cm from the fracture wall forms a zone in which there is a net consumption of CO_2 (the species CO_3^{2-} at this pH) by the reactions, while a net production of CO_2 occurs between about 1.7 and 4 cm from the fracture. CO_3^{2-} is produced at a distance of 2 cm from the fracture according to

$$CaMg(CO_3)_2 + 2\ OH^- \rightarrow CaCO_3 + Mg(OH)_2 + CO_3^{2-}, \quad (20)$$

in which Ca^{2+} and Mg^{2+} are conserved while CO_3^{2-} is produced. Evidently, the change in the local diffusive fluxes of Ca^{2+} and CO_3^{2-} changes the stoichiometry of the dolomite → calcite + brucite reaction. This behavior can be explained in the following way. Up to about 1.25 cm from the fracture, dolomite dissolves at its far from equilibrium rate of 1×10^{-7} mol m^{-3} s^{-1}. In this region, the flux of Ca^{2+} exceeds the rate at which dolomite can dissolve. The rate at which the reaction proceeds, therefore, is limited by the availability of CO_3^{2-}. Further into the rock matrix at about 2 cm from the fracture, the Ca^{2+} flux is much less because it is consumed by the reactions taking place in the zone closer to the fracture wall. As a result, CO_3^{2-} is produced according to Eqn. 20, and Ca^{2+} rat :r than CO_2 becomes the rate-limiting constituent. The e..cess CO_3^{2-} produced at 2 cm diffuses back toward the fracture wall and reacts with the excess Ca^{2+} at about 1.55 cm from the fracture.

The observations concerning the reaction stoichiometry outlined above indicate that the flux of Ca^{2+} into the rock matrix and the rate of dolomite dissolution are the two possible rate-limiting steps in the carbonate reactions. If dolomite dissolution occurred close to equilibrium (in which case the diffusive flux of Ca^{2+} would everywhere be the rate-limiting process), then the entire calcite precipitation profile should collapse into a single peak at the position marking the dolomite dissolution front (at $x = 0$ for early times). The observations imply that a decrease in the Ca^{2+} flux into the marl should also cause the calcite precipitation peak driven by Ca^{2+} and CO_3^{2-} interdiffusion to change its position. A rate limitation based on dolomite kinetics or the Ca^{2+} flux also suggests that the results are not sensitive to the rate constant for calcite precipitation. This has been verified by carrying out a simulation identical to that described above, except for the use of a rate constant for calcite of 1×10^{-8} mol m^{-2} s^{-2}. The slower calcite rate (not shown here) resulted only in a slight decrease in the sharpness of the calcite peak without changing its position at about 1.55 cm from the fracture wall.

This interdiffusion phenomenon explains the difference in the topologies of the reaction rate profiles for advective-dominant (high Peclet number) and pure diffusive transport, both

of which are shown in Fig. 5. In the case of advection, any excess of Ca^{2+} over and above the amount needed to precipitate calcite with the CO_3^{2-} provided by far from equilibrium dolomite dissolution reaction simply moves on downstream without reacting. Any CO_3^{2-} produced downstream by a change in the reaction stoichiometry, of course, has no way of affecting the reactions upstream when the transport is advective-dominant. In the case of pure diffusive transport, however, the CO_3^{2-} produced by reactions may diffuse back toward the fracture wall and react with the excess Ca^{2+} in that region. The differing topologies of the reaction rate profiles, therefore, are a natural consequence of the differing characters of advective and diffusive transport.

The difference between the reaction profiles in the case of advective vs. diffusive transport is not a trivial one here, since the calcite precipitation peak at about 1.55 cm from the fracture wall accounts for the bulk of the porosity change in the marl (Fig. 6). In contrast, the porosity reduction in the pure advective case investigated by LICHTNER and EIKENBERG (1994) is due primarily to the precipitation of various CSH phases. In the pure diffusion case, CSH phases (of which katoite and foshagite are volumetrically the most important) along with brucite do cause a substantial reduction in the marl's porosity between about 2 mm and 14 mm from the fracture, but the local precipitation of calcite due to the interdiffusion phenomenon described above dominates the reduction in porosity. Since the porosity is not updated in the diffusion and reaction equations, it takes on nonphysical negative values after about 15 years. As discussed above,

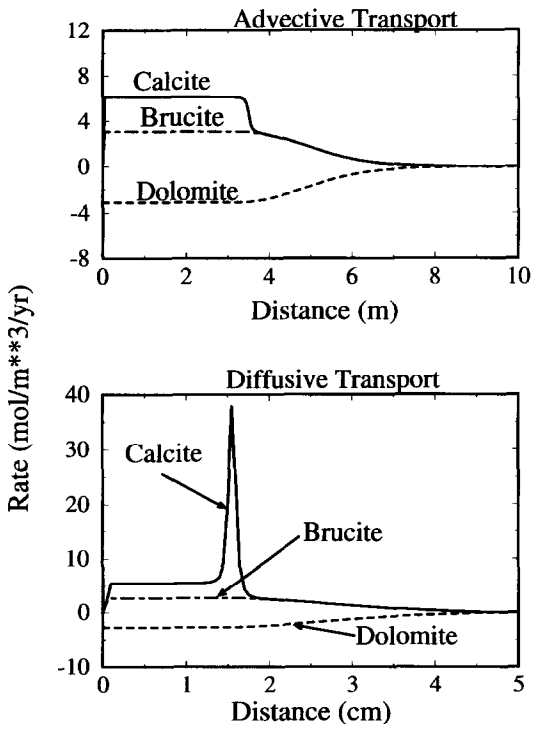

FIG. 5. Comparison of the topologies of the reaction rate profiles for advective (Peclet number = 100, Darcian flux = 1 m/y) and pure diffusive transport. Calculations assume a constant porosity in the transport equations.

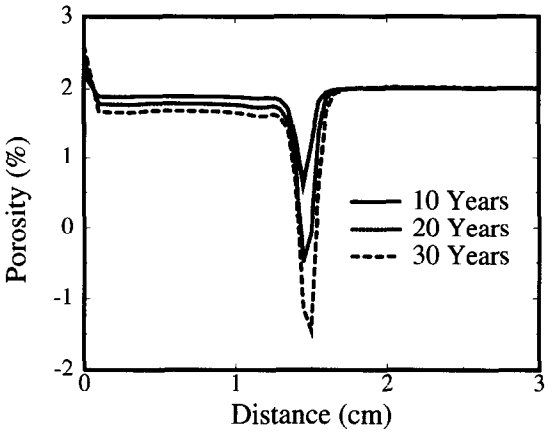

FIG. 6. Porosity evolution obtained if the mineral volume fractions are summed according to Eqn. 16. The porosity is "hypothetical", however, since the porosity which appears in the reaction-transport equations is assumed to remain constant in this calculation. Nonphysical, negative porosities, therefore, occur after about 15 years. The rapid porosity decrease close to 1.5 cm from the fracture is due primarily to calcite precipitation resulting from interdiffusion of Ca^{2+} and CO_3^{2-}. Note the porosity increase immediately adjacent to the fracture.

however, one can view these calculations as approximate representations of the case in which a dilation of the rock matrix compensates for the cementation of the rock by secondary phases. A rigorous treatment of this limiting case,

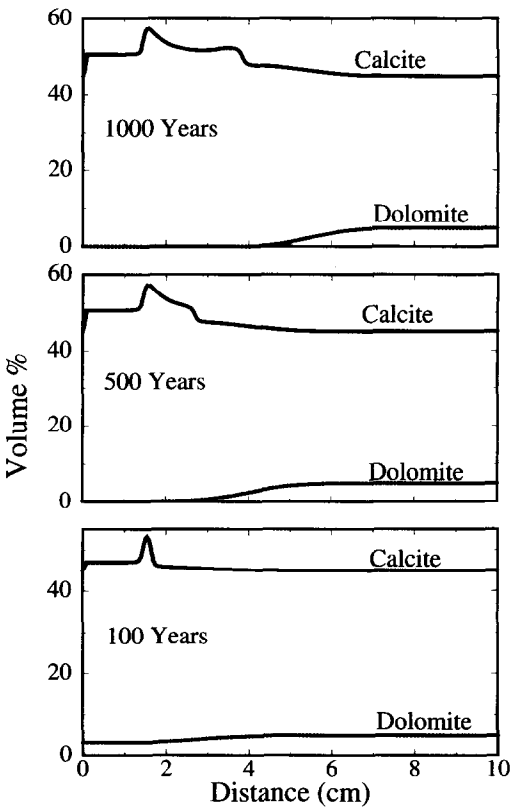

FIG. 7. Time evolution of the volume percentages of calcite and dolomite. Calculations assume a constant porosity in the transport equations.

however, would require that the minerals in the rock must also be transported mechanically in order to maintain a constant porosity. In addition to the porosity reduction within the rock matrix, the calculations also predict a porosity increase in the marl immediately adjacent to the fracture. This effect is also seen in the pure advective calculations (LICHTNER and EIKENBERG, 1994) and could result in an increase in the permeability of the fractured rock by widening the fractures.

The time evolution of the volume percentages of calcite and dolomite, obtained by integrating the reaction rates up to 1,000 years, is shown in Fig. 7. Note that the dolomite dissolution front has propagated about 4 cm away from the fracture wall by 1,000 years. The propagation of the dolomite front in turn causes a migration in the calcite precipitation peak with time, yielding the more complicated pattern in its volume percentage profile at 1,000 as compared to 100 years.

The precipitation rates of brucite, katoite, foshagite, and sepiolite within 10 cm of the fracture wall are shown in Fig. 8. In addition to calcite, these are the only phases to precipitate in significant amounts within this region. Katoite, foshagite, and sepiolite are close to equilibrium, so their rates of formation are limited primarily by the dissolution rates of quartz,

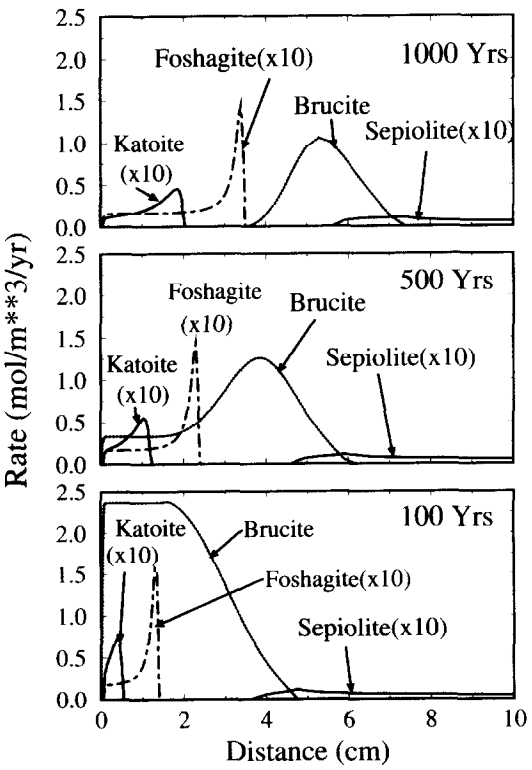

FIG. 8. Precipitation rates of brucite, sepiolite, foshagite, and katoite within 10 cm of the fracture wall at times of 100, 500, and 1,000 years. All of the rates except for that of brucite are multiplied by 10 to make them visible. Note the gradual propagation of the brucite precipitation peak away from the fracture wall as it follows the dolomite dissolution front. Note also that the amplitude of the precipitation peaks gradually decreases with increasing distance from the fracture wall, a result of the $t^{1/2}$ dependence of diffusion-driven reaction fronts. The calculation assumes a constant porosity in the transport equations.

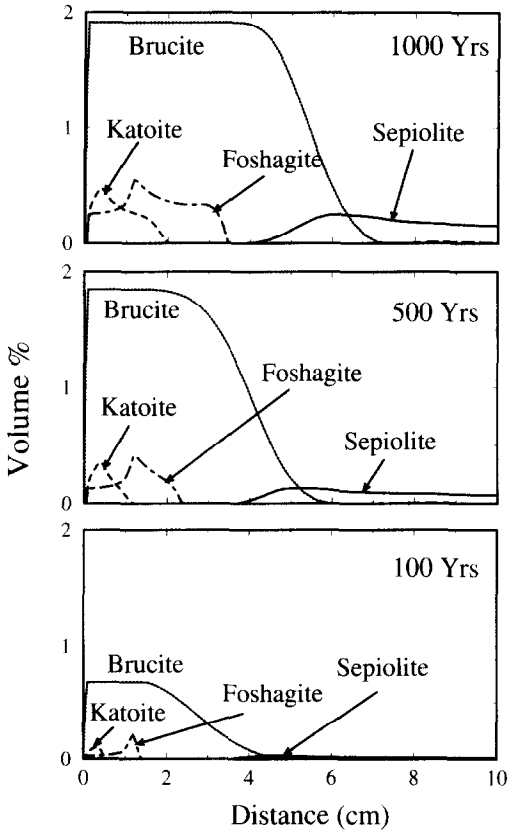

FIG. 9. Time evolution of the volume percentages of minor phases within 10 cm of the fracture wall. The calculation assumes a constant porosity in the transport equations.

muscovite, and kaolinite which provide the silica for the CSH phases. Small amounts of gibbsite, analcime, and natrolite (not shown) precipitate at about 8, 20, and 15 cm, respectively, from the fracture wall. The amplitude of the precipitation peaks decrease as they propagate away from the fracture wall. This is a feature of diffusion-driven metasomatism, where one expects a square root time dependence. When the reaction rates are integrated over time, they yield volume percent profiles as shown in Fig. 9. Note that over the first 2 cm of the diffusion profile, the percentage of brucite in the altered marl approaches a constant value. This is due to the fact that dolomite has been completely dissolved from the rock between 0 and 2 cm by 500 years (Fig. 7), thus removing the source of Mg which drives brucite precipitation.

Sensitivity to uncertainties in the reaction rates

The reaction rate constants for most of the minerals considered in this study are poorly known. Therefore, it is important to test the sensitivity of the results to uncertainties in the rate constants and/or the mineral surface areas. This is done by comparing two calculations in which all surface areas differ by two orders of magnitude. Although the results are not shown here, we have also tested the effect of using a smaller calcite rate constant as discussed above.

Figure 10 compares the solution pH profile at 500 years for two initial surface areas: 100 m^2 m^{-3} and 10,000

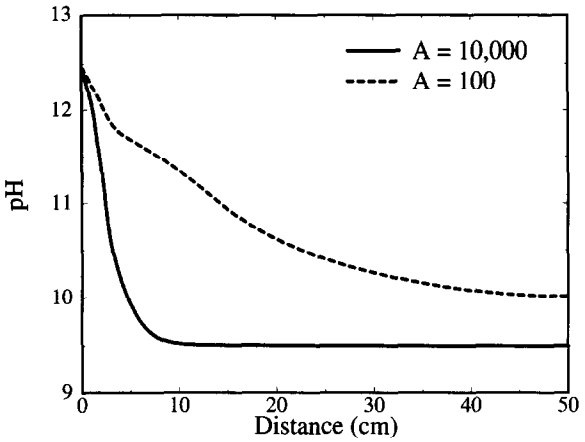

FIG. 10. Solution pH at 500 years using mineral reactive surface areas of 10,000 and 100 $m^2\ m^{-3}$. The calculation assumes a constant porosity in the transport equations.

$m^2\ m^{-3}$. The volume percentages of the minerals brucite, katoite, foshagite, and sepiolite for the two cases are shown in Fig. 11. As pointed out by LICHTNER (1993), both profiles could be obtained using only one surface area if the solutions are scaled in terms of both time and space. For the case of pure diffusive transport, the solutions for a field variable, F, (e.g., the solute concentration field or mineral volume fractions) scale according to

$$F(\sqrt{\sigma}x, \sigma t; k', D) = F(x, t; \sigma k', D), \qquad (21)$$

where σ is the scaling factor (in this case 100), k' is the effective rate constant including the surface area term, and D is the diffusion coefficient. In other words, the volume percentage profiles at 500 years over a length scale L for the case in which the reactive surface areas are 100 m^2 would be identical to the volume percentage profiles obtained from a calculation using 100 times larger rates if viewed at 5 years over a length scale $L/10$. This has been verified numerically for the case of pure diffusive transport using the code 1DREACT (results not shown here). Nonetheless, it is instructive to compare the results at the same time and over the same distance (i.e., without scaling), since the timescale of interest may be dictated by the time required for the radionuclides in the waste repository to decay to environmentally safe levels.

Note that the relative abundance of brucite and the CSH-phases katoite and foshagite in the two calculations differ, as they generally must since they are compared at the same times rather than at the times scaled according to Eqn. 21. In the case where the larger mineral surface areas are used, therefore, the entire process is more advanced and one would have to compare these results with the results obtained at 50,000 years, $L = 50$, and $A = 100$ m^2 to see equivalent spatial distributions of the minerals.

The results of the calculations are primarily sensitive to the rate constants and mineral surface areas used for dolomite and the silicate phases. In other words, the rate-limiting processes, in addition to the flux of species into the rock, are the dissolution of the primary minerals in the rock matrix. As pointed out by STEEFEL and VAN CAPPELLEN (1990), however, this might not be the case if nucleation kinetics were more rigorously included in the calculations. It is important, therefore, to keep these assumptions in mind when comparing these calculations with field and/or experimental observations.

Calculations with Porosity Feedback

The constant porosity calculations described above are appropriate if expansion of the rock keeps mineral precipitation from reducing the porosity. In the event that the rock matrix is immobile, however, the calculations become increasingly inaccurate with time as porosity decreases. Where porosity reduction occurs, the effective diffusion coefficient should decrease as well because of its porosity dependence (Eqn. 7), which in turn affects the solute concentration profiles.

In the calculations which follow, the porosity is updated after each time step using Eqns. 15 and 16, but otherwise are identical to the previous calculations. Cementation exponents of 1.25, 1.5, and 2 are used. The porosity evolution of the system for these three cementation exponents is shown in Fig. 12 up to 500 years. For the case in which the cementation exponent is taken as 1.5, the porosity approaches zero at approximately 1.4 cm from the fracture after about 15 years primarily because of the calcite precipitation peak discussed above (compare with Fig. 6). By 100 years, the porosity is reduced to about 1.1% in the region between 0.1 and 1.3 cm because of the precipitation of brucite and the CSH phases katoite and foshagite. Note that a porosity increase occurs at the fracture and extends out 1 mm into the rock matrix. The porosity evolution predicted with cementation exponents of 1.25 and 2.0 are also shown in Fig. 12. The use of differing cementation exponents changes both the rate at which the porosity reduction takes place and the position of sharpest porosity reduction. Both of these effects are the result of the

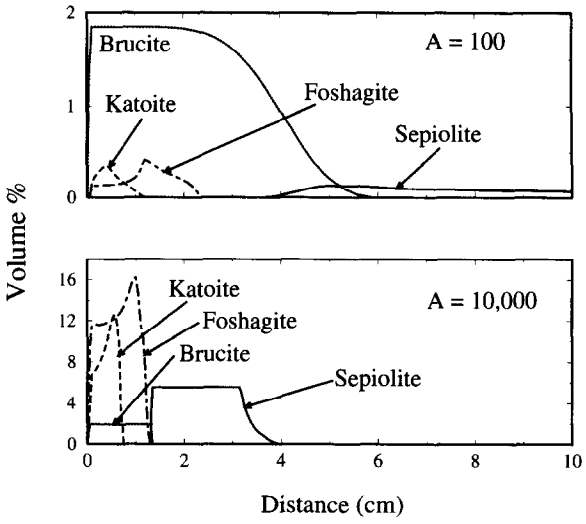

FIG. 11. Volume percentages of the secondary phases brucite, foshagite, katoite, and sepiolite within 10 cm of fracture wall at 500 years. The calculations differ only in assuming initial mineral reactive surface areas of 10,000 and 100 $m^2\ m^{-3}$. The calculation assumes a constant porosity in the transport equations.

changes in the magnitude of the effective diffusion coefficient (see Eqn. 7).

The local reduction in the porosity causes a decrease in the effective diffusion coefficient because of its porosity dependence. The evolution of the solution pH for the case in which a cementation exponent of 1.5 is assumed is shown in Fig. 13 between 10 and 500 years (compare with Fig. 3). A discontinuity develops in the pH profile, indicating that the porosity reduction (and the resulting decrease in the local diffusion coefficient) has caused the region immediately adjacent to the fracture to become isolated chemically from the marl beyond the cemented zone. Nonreactive solutes show the same discontinuity. As this process is followed out to longer times, the pH profile continues to evolve in the region between the completely cemented zone at about 1.4 cm and the fracture due to the continued porosity reduction in this region. Porosity reduction continuously sharpens the pH front, thus limiting the potential pH neutralization effects of the marl on fluid moving through the fracture.

The porosity decrease at 1.4 cm has a strong effect on reaction rate profiles in the rock matrix. Figure 14 shows the reaction rates of various minerals at 500 years, again for a cementation exponent of 1.5. Note that by 500 years, the pronounced calcite precipitation peak resulting from the interdiffusion of Ca^{2+} and CO_3^{2-} has disappeared. This is because the cementation of the zone at about 1.4 cm has effectively shut off the interdiffusion mechanism; that is, CO_3^{2-} can no longer diffuse in from the region beyond 1.4 cm from the fracture. In addition, marked discontinuities develop in the rates of the other reacting phases. Katoite and foshagite precipitate in the 0–1.4 cm region, while sepiolite precipitates in the region beyond 1.4 cm.

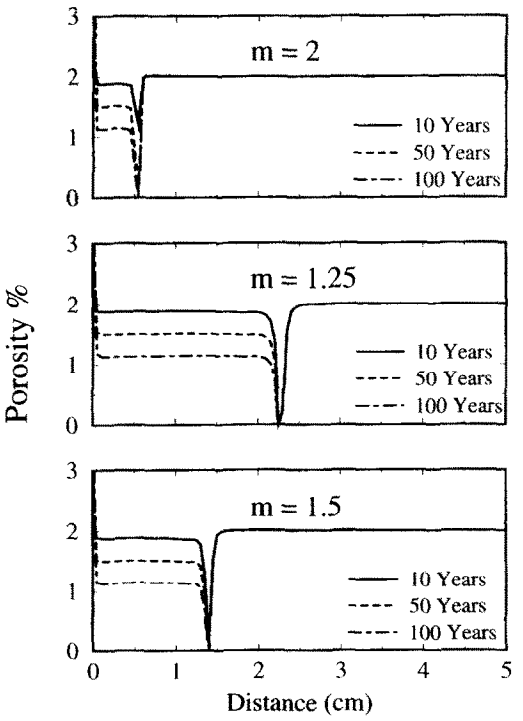

FIG. 12. Porosity evolution for cases in which the cementation exponent, m, is assumed to be 1.5, 1.25, and 2 (see Eqn. 7). Mineral precipitation and dissolution reactions are assumed to modify the porosity which appears in the transport equations.

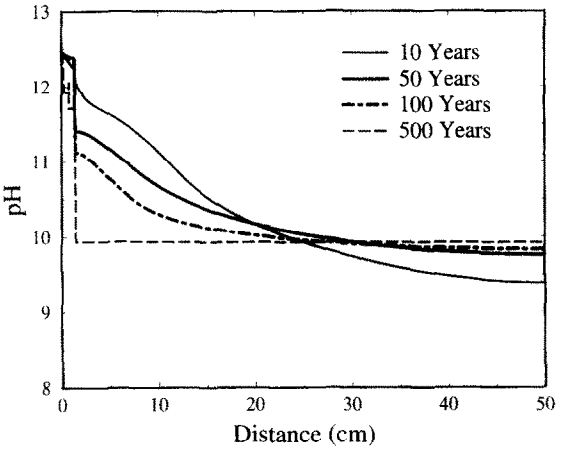

FIG. 13. Time evolution of the solution pH for calculation in which mineral precipitation and dissolution reactions modify the porosity which appears in the transport equations. Note the development of a discontinuity at about 1.5 cm from the fracture due to the local reduction in the diffusion coefficient according to Eqn. 7. The cementation of this zone prevents ions from diffusing through the zone and thus effectively isolates the region beyond 1.5 cm chemically from the region adjacent to the fracture wall. A cementation exponent of 1.5 is assumed.

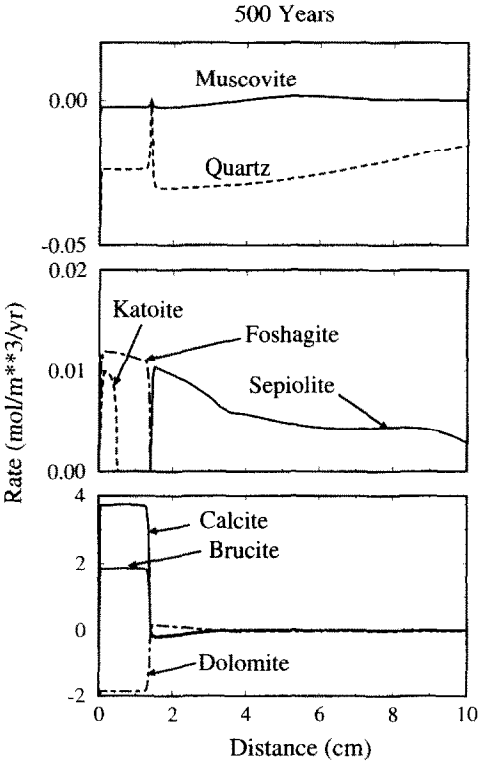

FIG. 14. Reaction rates at 500 years for calculation in which a porosity feedback in the transport equations is included. Note the discontinuity in the reaction rates which develops where the porosity goes to 0 at about 1.5 cm from the fracture. A cementation exponent of 1.5 is assumed.

Table 6. Solute concentrations and constraints for the high Na-K cement pore water used as a boundary condition in the calculations. High Na and K values are assumed to be derived from dissolution of cement.

	Concentration (mol/l)	Constraint
OH^-	2.71×10^{-1}	charge balance
$Al(OH)_4^-$	1.11×10^{-4}	katoite
K_{tot}	2.0×10^{-1}	dissolution of cement
Na_{tot}	1.0×10^{-1}	dissolution of cement
Ca^{2+}	3.57×10^{-4}	portlandite
Mg^{2+}	1.65×10^{-10}	brucite
$SiO_{2(aq)}$	8.44×10^{-10}	foshagite
CO_3^{2-}	1.14×10^{-4}	calcite
SO_4^{2-}	4.27×10^{-3}	ettringite
Cl_{tot}	1.03×10^{-3}	marl groundwater
T(°C)	25	
I(M)	2.87×10^{-1}	
pH	13.26	

High Na + K Cement Porewaters

The calculations presented above have all assumed a constant fluid composition in the fracture characterized by relatively low Na and K concentrations (Table 1). A porewater reacted for short times with cement (e.g., <10,000 years), however, may have much higher NaOH and KOH concentrations and therefore considerably higher pH values. If equilibrium between the porewater and portlandite is assumed to hold in the cement, then the higher OH^- concentrations in the fluid will also result in lower Ca^{2+} concentrations. To examine some of the possible effects of cement porewaters with higher concentrations of Na and K and with higher pH values, we consider two separate scenarios. In the first scenario, the composition of the cement porewaters remains constant at the values given in Table 6 over the 1,000 years of the simulation. In the second scenario, time-dependent boundary concentrations are used to represent the gradual depletion in Na and K over 1,000 years (e.g., BERNER, 1992). In both cases porosity reduction is coupled to the effective diffusion coefficients.

For the time-dependent case it is assumed that, as marl groundwater flows through the repository leaching alkalies from the cement, the concentration of alkali in solution decreases exponentially with time according to a first order rate law as the inventory of alkalies in the cement is depleted. Thus, the total alkali concentration in the cement pore solution, $\Psi_j^0(t)$, is assumed to obey the expression

$$\Psi_j^0(t) = (\hat{\Psi}_j^0 - \Psi_j^{gw})e^{-\lambda_j t} + \Psi_j^{gw}, \qquad (22)$$

with j = Na, K, where $\hat{\Psi}_j^0$ represents the initial cement pore solution composition, Ψ_j^{gw} represents the ambient marl groundwater concentration, and λ_j denotes the decay constant. By taking the ratio of the initial inventories, an expression is obtained for the ratio of the Na and K decay constants (LICHTNER and EIKENBERG, 1994):

$$\frac{\lambda_{Na}}{\lambda_K} = \frac{M_{Na}^0}{M_K^0}\frac{W_K}{W_{Na}}\frac{(\hat{\Psi}_K^0 - \Psi_K^{gw})}{(\hat{\Psi}_{Na}^0 - \Psi_{Na}^{gw})}, \qquad (23)$$

where W_j represents the gram-formula-weight of the jth species and M_j^0 is the initial inventory of the jth alkali in the cement. To determine values for the decay constants λ_{Na} and λ_K, it is assumed that the mass ratio Na:K in the cement is 1:10, and the molar ratio in the pore solution is 1:2 (BERNER,

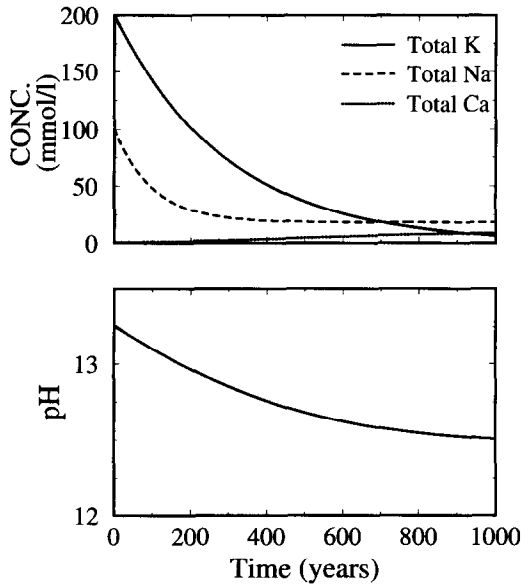

FIG. 15. Time evolution of the total Na and K concentrations, $\Psi_{Na}^0(t)$ and $\Psi_K^0(t)$, in the fracture for the case where transient, incongruent dissolution of the cement is assumed to occur.

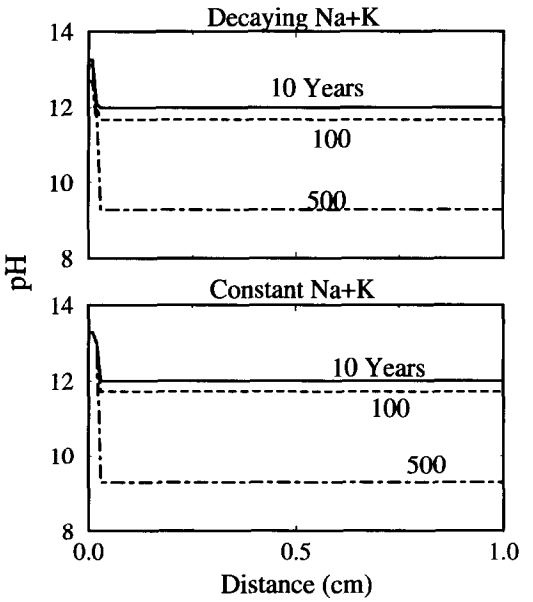

FIG. 16. Solution pH for the cases in which the total concentrations of Na and K in the fracture are assumed to decay with time (see Fig. 15) and for the case of a constant concentration of 0.2 and 0.1 molar K and Na, respectively. Note that in the case of the decaying Na and K concentrations, the solution pH at the fracture wall (x = 0) decreases with time as well. A porosity feedback in the transport equations is included.

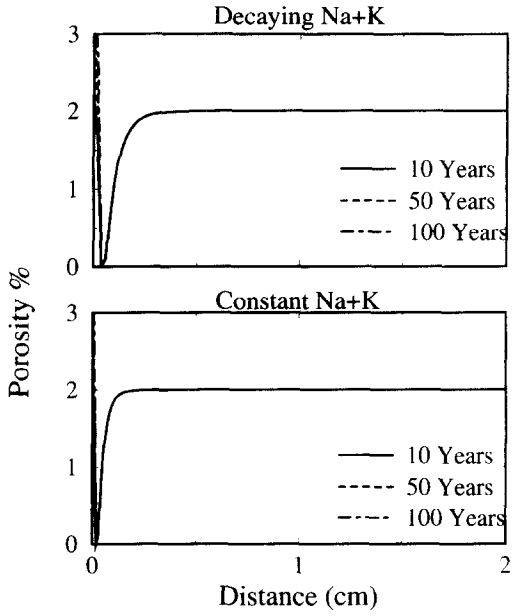

FIG. 17. Porosity evolution for the cases of gradually decaying and constant, high Na and K concentrations in the fracture.

1990). If an arbitrary value for $\lambda_{Na} = 10^{-2}$ y^{-1} is selected yielding a half-life of approximately 69.3 years, this gives $\lambda_K = 0.0034$ y^{-1} or a half-life of approximately 203.8 years. We use the values given in Table 6 for the initial total concentrations of K and Na, $\tilde{\Psi}^0_K$ and $\tilde{\Psi}^0_{Na}$, and we use the values in Table 1 for the groundwater concentrations, Ψ^{gw}_K and Ψ^{gw}_{Na}. Using Eqn. 22, one obtains the total concentrations of K and Na in the fracture as a function of time. These calculated values are shown in Fig. 15. The pH of the resulting solution and the remaining species concentrations are calculated by equilibrating the solution at each instant with the same minerals used for the calcium hydroxide solution described above.

The time variation of the solution pH within the marl matrix for the two cases (constant and time-dependent (Na + K) is shown in Fig. 16. Note that the two cases are very similar except for the gradual decrease in the pH of the pore fluids in the fracture (at $x = 0$) which occurs in the calculation with a decaying (Na + K) concentration. A distinct discontinuity in the pH develops in both cases because of local porosity reduction. The evolution of the porosity is shown in Fig. 17 for the two cases. In both cases, the porosity in the rock matrix goes to zero within as little as 10 years a very short distance from the fracture wall. The porosity reduction, as in the low-(Na + K) case considered above, results from the interdiffusion of Ca^{2+} and CO_3^{2-} which drives calcite precipitation. This reaction is linked to the pH and the Na + K concentrations in the fracture only in so far as these concentrations influence the Ca^{2+} in the fracture. As predicted above, the lower Ca^{2+} concentrations in the fracture which occur when the (Na + K) concentrations are higher (Table 6) result in a reduced diffusive flux of Ca^{2+} into the rock matrix, thus shifting the location of the calcite precipitation peak. The lower Ca^{2+} flux, therefore, causes diffusion to become the rate-limiting process within a very short distance of the fracture wall. At any distance greater than 0.5 mm from the fracture wall, Ca^{2+} is conserved and CO_3^{2-} is produced in the reaction dolomite → calcite + brucite which proceeds according to Eqn. 20. The effect of differing Ca^{2+} fluxes into the rock matrix can be seen in Fig. 18 where we have plotted the calcite precipitation rate for three different (Na + K) concentrations in the fracture. Where the (Na + K) = 0.3 M (the fluid composition given in Table 6), the calcite precipitation peak forms immediately adjacent to the fracture.

DISCUSSION

A marl rock matrix adjacent to a hyperalkaline fluid-filled fracture could be completely cemented locally in as little as 10 to 500 years. All the calculations predict a narrow zone (on a millimeter scale) immediately adjacent to the fracture wall where the porosity increases, and a zone on the order of millimeters to centimeters from the fracture where the porosity tends to zero. These results assume that the fracture remains open and is continually flushed with the hyperalkaline fluid emanating from the cement.

Implications for Modeling of Water-Rock Interaction

The calculations presented here, although applied to a specific environmental problem, have some significant implications for the applicability of various geochemical models to water-rock interaction. The calculations indicate that significant differences may exist in the geochemical behavior of systems characterized by advective vs. diffusive transport, aside from the inherent difference in the length scales involved. The most significant difference is that the pure diffusion calculations predict calcite will precipitate locally due to interdiffusion of Ca^{2+} and CO_3^{2-}. This local precipitation accounts for most of the porosity reduction predicted for the marl rock matrix and is therefore potentially a nontrivial effect. The interdiffusion effect is particularly important for

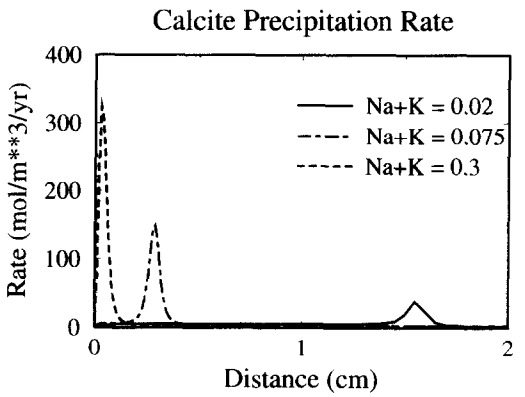

FIG. 18. Calculated calcite precipitation rate as a function of various total Na + K concentrations in the fracture. Because of the constraints that the fluid in the fracture be at equilibrium with respect to calcite and portlandite, increased Na and K concentrations result in higher pH values and lower Ca concentrations. The lower Ca concentrations in the fracture result in a reduced diffusive flux of Ca into the rock matrix, thus causing the calcite precipitation peak to migrate in toward the fracture wall. See text for further discussion.

the case where the cement porewaters have high Na and K concentrations and high pH (>13), since in this case the porosity reduction resulting from the interdiffusion phenomenon greatly exceeds the porosity reduction due to other precipitation reactions. In the case of a high Na + K cement porewater, therefore, an even greater discrepancy between advective-dominant and diffusive transport is apparent. A "reaction path" calculation, which is ultimately based on an assumption that either the system is closed or that transport is purely advective (STEEFEL and LASAGA, 1992), will also fail in describing a system where diffusive transport dominates.

An analysis based on the Peclet number ($Pe = vl/D$) suggests that there is some length scale, l, where advective transport dominates over diffusive and/or dispersive transport. This conclusion applies in a straightforward way to transport through a homogeneous porous medium. Because there are natural length scales characterizing fractured rock, a scaling analysis such as that given by Eqn. 21 cannot be carried out. It may be that in rock containing fractures separated by finite distances, diffusive transport could have a very important effect on the kind and spatial distribution of reaction products no matter what the overall size of the system.

Implications for the Migration Rate of Contaminants

The predicted mineral reactions may have several possible implications for the rate of migration of contaminants. One possibility, which is directly addressed by the calculations, is that mineral precipitation reduces the porosity of the rock matrix. By decreasing the effective diffusion coefficient in the marl, the porosity reduction may isolate the fracture chemically and physically from the rock matrix (NERETNIEKS, 1980). The problem of contaminant retardation by matrix diffusion was discussed by NERETNIEKS (1980) and TANG et al. (1981). NOVAK and SEVOUGIAN (1993) show the combined effect of physical retardation via matrix diffusion and chemical retardation due to mineral precipitation in a dual porosity system. None of these studies, however, considered porosity change. Another possibility, not considered in the calculations, is that the force of crystallization in the marl could cause the alteration zone to dilate, thus closing the fracture itself. In this case, the marl rock matrix could maintain a finite porosity, while the permeability of the fracture system developed in the marl would tend to decrease. We consider some of the potential implications of both scenarios below.

A reduction in the effective diffusion coefficients of solutes in the rock matrix bordering a fracture increases the rate of both reactive and nonreactive contaminant migration down the fracture (NERETNIEKS, 1980; TANG et al., 1981; NOVAK and SEVOUGIAN, 1993). Contaminants are physically retarded through matrix diffusion because the diffusion in the rock matrix represents a "diffusive loss" from the fracture. The reduction in the porosity of the rock matrix might have an even greater effect on a reactive contaminant. If a contaminant cannot diffuse a significant distance into the rock matrix bordering a fracture, then the total reactive surface area which is available for both precipitation/dissolution and sorption reactions is decreased. "Armoring" of the fracture, then, might reduce the neutralizing and sorbing capacity of the rock. In contrast, newly precipitated material along or near the fracture wall may have a very high specific surface area which could enhance sorption, thus reversing to some extent the effects of porosity reduction in the rock matrix.

The calculations above also predict that the reactions change the relative abundance of minerals in the region bordering the fracture. The infiltration of a highly reactive fluid emanating from a cement-bearing waste repository can significantly alter the geochemical properties of the host rock, even if no physical changes take place. To assess the relative importance of changes in the modal mineralogy of the rock matrix vs. the reduction in the porosity of the matrix, one would have to carry out calculations including the specific contaminant or contaminants of interest. In nature, however, the "armoring" effect might be even more extreme, since precipitation of relatively small quantities of secondary minerals could coat the surfaces of the primary minerals in the rock, thus making them essentially unreactive. In the calculations presented here, it is assumed that a primary mineral is capable of reacting as long as it has a non-zero volume fraction. The rate at which the neutralization capacity of the rock is modified, therefore, may be underestimated in the calculations.

An important feature of a groundwater flow system characterized by fracture-dominated flow is that selective armoring of the fracture walls can occur in much less time than would be required to completely alter a homogeneous porous medium. If this effect of selective rock alteration along fracture walls is compounded by the fact that the fluids emanating from the concrete repository are highly reactive because of their very high pH, then the time required to modify significantly the physical and chemical characteristics of the host rock may be very short, perhaps on the order of tens of years as suggested by the calculations presented here. Because of the uncertainty in the parameters used in the calculations, it is not possible to predict a definite time scale for the porosity reduction to occur. The calculations suggest, however, that the physical or chemical properties of the marl host rock will not remain constant for 500 years and perhaps not even for ten's of years.

A second possibility is that precipitation of secondary minerals might cause the rock matrix to expand, thus closing off the fractures. A local reduction in fracture aperture will result in a decrease in permeability, thus slowing the rate of contaminant transport. Permeability reduction in the fractures could also occur because of precipitation within the fracture itself, a process which is not explicitly considered in this study. Shutting off flow in the fracture, however, would allow the uncontaminated groundwater to diffuse back into the fracture and dissolve the fracture filling, thereby opening it once again to flow.

CONCLUSIONS

Reactive transport calculations are used to analyze water-rock interaction in rock matrix bordering fractures filled with a hyperalkaline fluid. The calculations indicate that diffusive

transport may result in markedly different reaction products from those likely to occur in the case of advective-dominant transport. Using a primary mineralogy which is analogous to the Cretaceous and Tertiary marls proposed by the Swiss as a low-level nuclear waste repository, the diffusion-reaction calculations suggest that complete cementation within centimeters of the fracture walls may occur in 10 to 500 years. The bulk of the porosity change in the case of diffusive transport is due to the precipitation of calcite as a result of interdiffusion of Ca^{2+} and CO_3^{2-}. In contrast, porosity reduction is less rapid in the case of advective-dominant transport since calcite precipitates only as a replacement of dolomite. Both diffusive and advective-dominant transport result in a porosity increase immediately adjacent to the fracture. These effects may occur before the radionuclides in the repository have decayed to safe levels.

When the porosity of the rock matrix is coupled to the effective diffusion coefficient in the marl, the calculations predict that the resulting cemented zone can cause the fracture to become chemically and physically isolated from the marl rock matrix. The calculations imply, therefore, that "armoring" of the fracture may substantially reduce the neutralizing and sorbing capacity of the marl by limiting both the physical and chemical retardation capacity of the rock matrix. The possible effects of a reduction in matrix porosity, however, must be weighed against the other potential phenomena resulting from mineral precipitation and dissolution reactions taking place in the rock matrix, including changes in modal mineralogy and the formation of precipitates with a high specific surface area. Although the uncertainties in many of the parameters used in the calculations make it difficult to establish a definite timescale, the calculations presented here suggest that further analyses of the migration behavior of the radionuclides in the vicinity of a cement-bearing waste repository need to take into account the chemical and physical changes to the host rock brought about by reaction with a hyperalkaline fluid. The problem also needs to be examined with the use of a dual porosity model, since it is not possible to establish how far and how rapidly the high pH plume can propagate without coupling diffusion and reaction in the rock matrix to fluid flow through the fractures.

Acknowledgments—We acknowledge the support of the Schweizerischer Nationalfonds in the form of a grant (21-30908.91) to Peter C. Lichtner which funded a 1 year postdoctoral position for the senior author at the Universität Bern in Switzerland. We are also grateful for the financial support of both authors by Professor Dr. Tjerk Peters of the Mineralogisch-Petrographisches Institut at the Universität Bern. The manuscript benefited considerably from careful reviews by Eric Oelkers, Philippe Van Cappellen, Russell Alexander, Ian McKinley, Enrique Merino, and David Sevougian.

Editorial handling: E. Merino

REFERENCES

AAGAARD P. and HELGESON H. C. (1982) Thermodynamic and kinetic constraints on reaction rates among minerals and aqueous solutions. I. Theoretical considerations. *Amer. J. Sci.* **282**, 237–285.

ATKINS M. and GLASSER F. P. (1992) Application of portlandite cement-based materials to radioactive waste immobilization. *Waste Mgmt.* **12**, 105–131.

ATKINSON A., HEARNE J. A., and KNIGHTS C. F. (1987) *Aqueous chemistry and thermodynamic modeling of CaO-SiO_2-H_2O gels.* AERE Report 12548. Harwell Laboratory, UK.

BALASHOV V. N. and LEBEDEVA M. I. (1991) Macrokinetic model of the origin and development of a monomineralic bimetasomatic zone. In *Progress in Metamorphic and Magmatic Petrology. A memorial volume in honor of D. S. Korzhinskii* (ed. L. L. PERCHUK), pp. 167–195. Cambridge Univ. Press.

BERNER U. R. (1987) Modeling pore water chemistry in hydrated cement. *Mat. Res. Soc. Symp. Proc.* **84**, 319–330.

BERNER U. R. (1990) *A thermodynamic description of the evolution of pore water chemistry and uranium speciation during the degradation of cement.* PSI Report 62 and NAGRA Technical Report NTB-91-12.

BERNER U. R. (1992) Evolution of pore water chemistry during degradation of cement in a radioactive waste repository environment. *Waste Mgmt.* **12**, 201–219.

BOUDREAU B. P. and CANFIELD D. E. (1993) A comparison of closed- and open-system models for porewater pH and calcite-saturation state. *Geochim. Cosmochim. Acta* **57**, 317–334.

BRADY P. V. and WALTER J. V. (1989) Controls on silicate dissolution rates in neutral and basic pH solutions at 25°C. *Geochim. Cosmochim. Acta* **53**, 2823–2830.

BRIMHALL G. H. (1977) Early fracture-controlled disseminated mineralization at Butte, Montana. *Econ. Geol.* **72**, 37–59.

BRYANT S. L., SCHECHTER S. L., and LAKE L. W. (1987) Mineral sequences in precipitation/dissolution waves. *Amer. Inst. Chem. Eng. J.* **33**, 1271–1287.

BUSEY R. H. and MESMER R. E. (1977) Ionization equilibrium of silicic acid and polysilicate formation in aqueous sodium chloride solutions to 300°C. *Inorg. Chem.* **16**, 2444–2450.

DULLIEN F. A. L. (1979) *Porous Media.* Academic Press.

EIKENBERG J. (1990) *On the problem of silica solubility at high pH.* NAGRA Technical Report NTB-90-36.

FELMY A. R. and WEARE J. H. (1991) Calculation of multicomponent ionic diffusion from zero to high concentration: I. The system Na–K–Ca–Mg–Cl–SO_4–H_2O at 25°C. *Geochim. Cosmochim. Acta* **55**, 113–131.

FRANTZ J. D. and MAO H. K. (1976) Bimetasomatism resulting from intergranular diffusion: I. A theoretical model for monomineralic reaction zone sequences. *Amer. J. Sci.* **276**, 817–840.

FRANTZ J. D. and MAO H. K. (1979) Bimetasomatism resulting from intergranular diffusion: II. Prediction of multimineralic zone sequences. *Amer. J. Sci.* **279**, 302–323.

GLASSER F. P., MACPHEE D., and LACHOWSKI E. E. (1988) Modeling approach to the prediction of equilibrium phase distribution in slag-cement blends and their solubility properties. *Mat. Res. Soc. Symp. Proc.* **112**, 3–12.

GREENBERG S. A. and CHANG T. N. (1965) Investigation of the hydrated calcium silicates II. Solubility relationships in the calcium oxide-silica-water system at 25°C. *J. Phys. Chem.* **69**, 1151–1173.

GREENBERG S. A. and PRICE E. W. (1957) The solubility of silica in solutions of electrolytes. *J. Phys. Chem.* **61**, 960–965.

GUY B. (1993) Mathematical revision of Korzhinskii's theory of infiltration metasomatic zoning. *Eur. J. Mineral.* **5**, 317–339.

HINDMARSH A. C. (1977) *Solution of block-tridiagonal systems of linear algebraic equations.* University California Internal Document 30150.

KALOUSEK G. L. (1952) Application of differential thermal analysis in a study of the system lime-silica-water. *Proc. 3rd Intl. Symp. on Chemistry of Cements, London.*

KHOURY H. N. and NASSIR S. (1982) High-temperature mineralization in the bituminous limestone in Maqarin area—North Jordan. *Neus Jahro Mineral.* **144**, 197–213.

KHOURY H. W., SALAMEH E., and ABDUL-JAHR Q. (1985) Characteristics of an unusual highly alkaline water from the Maqarin area, Northern Jorndan. *J. Hydrol.* **81**, 79–91.

KIRKNER D. J. and REEVES H. (1988) Multicomponent mass transport with homogeneous and heterogeneous chemical reactions: Effect of chemistry on the choice of numerical algorithm. I. Theory. *Water Resources Res.* **24**, 1719–1729.

KORZHINSKII D. S. (1970) *Theory of Metasomatic Zoning* (trans. J. AGRELL). Oxford Univ. Press.

LASAGA A. C. (1979) The treatment of multi-component diffusion and ion pairs in diagenetic fluxes. *Amer. J. Sci.* **279,** 324–346.

LASAGA A. C. (1981) Rate laws in chemical reactions. In *Kinetics of Geochemical Processes* (ed. A. C. LASAGA and R. J. KIRKPATRICK); *Rev. Mineral.* **8,** 135–169.

LASAGA A. C. (1984) Chemical kinetics of water-rock interactions. *J. Geophys. Res.* **89,** 4009–4025.

LEA F. M. (1970) *The Chemistry of Cement and Concrete.* Edward Arnold Ltd.

LICHTNER P. C. (1985) Continuum model for simultaneous chemical reactions and mass transport in hydrothermal systems. *Geochim. Cosmochim. Acta* **49,** 779–800.

LICHTNER P. C. (1988) The quasi-stationary state approximation to coupled mass transport and fluid-rock interaction in a porous medium. *Geochim. Cosmochim. Acta* **52,** 143–165.

LICHTNER P. C. (1991) The quasi-stationary state approximation to fluid/rock reaction: Local equilibrium revisited. In *Diffusion, Atomic Ordering, and Mass Transport; Advances in Physical Geochemistry* (ed. J. GANGULY), Vol. 8, pp. 454–562.

LICHTNER P. C. (1992) Time-space continuum description of fluid/rock interaction. *Water Resources Res.* **28,** 3135–3155.

LICHTNER P. C. (1993) Scaling properties of time-space kinetic mass transport equations and the local equilibrium limit. *Amer. J. Sci.* **293,** 257–296.

LICHTNER P. C. and EIKENBERG J. (1994) Propagation of a hyperalkaline plume into the geological barrier surrounding a radioactive waste depository. NAGRA Tech. Rpt. NBT 93-16, 579.

LICHTNER P. C., OELKERS E. H., and HELGESON H. C. (1986) Interdiffusion with multiple precipitation/dissolution reactions: Transient model and the steady-state limit. *Geochim. Cosmochim. Acta* **50,** 1951–1966.

LIU C. W. and NARASIMHAN T. N. (1989a) Redox-controlled multiple-species reactive chemical transport. 1. Model development. *Water Resources Res.* **25,** 869–882.

LIU C. W. and NARASIMHAN T. N. (1989b) Redox-controlled multiple-species reactive chemical transport. 2. Verification and application. *Water Resources Res.* **25,** 883–910.

MARSILY G. DE (1986) *Quantitative Hydrogeology.* Academic Press.

MERINO E., NAHON D., and WANG Y. (1993) Kinetics and mass transfer of pseudomorphic replacement: Application to the replacement of parent minerals and kaolinite by Al, Fe, and Mn oxides during weathering. *Amer. J. Sci.* **293,** 135–155.

MEYER C. and HEMLEY J. J. (1967) Wall rock alteration. In *Geochemistry of Hydrothermal Ore Deposits* (ed. H. L. BARNES), pp. 166–235. Holt, Rinehart, and Winston.

MEYER C. et al. (1968) Ore deposits at Butte, Montana. In *Ore Deposits of the U.S., 1933–1967* (ed. J. D. RIDGE), 1373–1416. Am. Inst. Min. Eng.

NERETNIEKS I. (1980) Diffusion in the rock matrix: An important factor in radionuclide retardation? *J. Geophys. Res.* **85,** 4379–4397.

NOVAK C. F. and SEVOUGIAN S. D. (1993) Propagation of dissolution/precipitation waves in porous media. In *Migration and Fate of Pollutants in Soils and Subsoils* (ed. D. PETRUZZELLI and F. G. HELFFERICH); *NATO ASI Series. Series G: Ecological Sciences* **32,** pp. 275–307. Springer-Verlag.

NOVAK C. F., SCHECHTER R. S., and LAKE L. W. (1989) Diffusion and solid dissolution/precipitation in permeable media. *Amer. Inst. Chem. Eng. J.* **35,** 1057–1072.

OELKERS E. H. and HELGESON H. C. (1988) Calculation of the thermodynamic and transport properties of aqueous species at high pressures and temperatures: Aqueous tracer diffusion coefficients of ions to 1,000°C and 5 kb. *Geochim. Cosmochim. Acta* **52,** 63–85.

ORTOLEVA P., CHADAM J., MERINO E., and SEN A. (1987) Geochemical self-organization. II: The reactive-infiltration instability. *Amer. J. Sci.* **287,** 1008–1040.

PATANKAR S. V. (1980) *Numerical Heat Transfer and Fluid Flow.* Hemisphere Publ.

REARDON E. J. (1992) Problems and approaches to the prediction of the chemical composition in cement/water systems. *Waste Mgmt.* **12,** 221–239.

REED M. H. (1982) Calculation of multicomponent chemical equilibria and reaction processes in systems involving minerals, gases, and an aqueous phase. *Geochim. Cosmochim. Acta* **46,** 513–528.

SALES R. H. and MEYER C. (1948) Wallrock alteration at Butte, Montana. *Amer. Inst. Mineral. Eng. Trans.* **178,** 9–35.

SALES R. H. and MEYER (1949) Results from preliminary studies of vein formation at Butte, Montana. *Econ. Geol.* **44,** 465–484.

SALES R. H. and MEYER C. (1950) Interpretation of wallrock alteration at Butte, Montana. *Colo. Sch. Mines Quart.* **45,** 261–274.

SANFORD W. E. and KONIKOW L. F. (1989) Simulation of calcite dissolution and porosity changes in saltwater mixing zones in coastal aquifers. *Water Resources Res.* **25,** 655–667.

SARKAR A. K., BARNES M. W., and ROY D. M. (1982) *Longevity of borehole and shaft sealing materials: thermodynamic properties of cements and related phases applied to repository sealing.* Office of Nuclear Waste Isolation, Technical Report ONWI-201.

SCHECHTER R. S., BRYANT S. L., and LAKE L. W. (1987) Isotherm-free chromatography: Propagation of precipitation/dissolution waves. *Chem. Eng. Comm.* **58,** 353–376.

SEVOUGIAN S. D., SCHECHTER R. S., and LAKE L. W. (1993) The effect of partial local equilibrium on the propagation of precipitation/dissolution waves. *Ind. Eng. Chem. Res.,* **32,** pp. 2281–2304.

STEEFEL C. I. (1992) Coupled fluid flow and chemical reaction: Model development and application to water-rock interaction. Ph.D. thesis, Yale Univ.

STEEFEL C. I. and LASAGA A. C. (1990) Evolution of dissolution patterns: Permeability change due to coupled flow and reaction. In *Chemical Modeling in Aqueous Systems II* (ed. D. C. MELCHIOR and R. L. BASSETT); *ACS Symp. Ser. No. 416,* 212–225.

STEEFEL C. I. and LASAGA A. C. (1992) Putting transport into water-rock interaction models. *Geology* **20,** 680–684.

STEEFEL C. I. and LASAGA A. C. (1994) A coupled model for transport of multiple chemical species and kinetic precipitation/dissolution reactions with application to reactive flow in single phase hydrothermal systems. *Amer. J. Sci.* **294,** 529–592.

STEEFEL C. I. and VAN CAPPELLEN P. (1990) A new kinetic approach to modeling water-rock interaction: The role of nucleation, precursors, and Ostwald ripening. *Geochim. Cosmochim. Acta* **54,** 2657–2677.

TANG D. H., FRIND E. O., and SUDICKY E. A. (1981) Contaminant transport in fractured porous media: Analytical solutions for a single fracture. *Water Resources Res.* **17,** 555–564.

THORNTON S. D. and RADKE C. J. (1933) Dissolution and condensation kinetics of silica in alkaline solution. *Soc. Petrol. Eng. J.* (May), 743–752.

WALSH M. P., BRYANT S. L., SCHECTER R. S., and LAKE L. W. (1984) Precipitation and dissolution of solids attending flow through porous media. *Amer. Inst. Chem. Eng. J.* **30,** 317–327.

WEARE J. H., STEPHENS J. R., and EUGSTER H. P. (1976) Diffusion metasomatism and mineral reaction zones: General principles and application to feldspar alteration. *Amer. J. Sci.* **276,** 767–816.

WOLERY T. J., JACKSON K. J., BOURCIER W. L., BRUTON C. J., VIANI B. E., KNAUSS K. G., and DELANY J. M. (1990) Current status of the EQ3/6 software package for geochemical modeling. In *Chemical Modeling in Aqueous Systems II* (ed. D. C. MELCHIOR and R. L. BASSETT); *ACS Symp. Ser. No. 416,* 104–116.

YEH G. T. and TRIPATHI V. S. (1989) A critical evaluation of recent developments in hydrogeochemical transport models of reactive multichemical components. *Water Resources Res.* **25,** 93–108.

YEH G. T. and TRIPATHI V. S. (1991) A model for simulating transport of reactive multispecies components: Model development and demonstration. *Water Resources Res.* **27,** 3075–3094.

APPENDIX: NUMERICAL METHODS

The numerical method used to solve the set of partial differential equations given by Eqns. 4 and 15 is described in detail in STEEFEL and LASAGA (1994). A "one-step" or "global implicit" method is

used to solve the equations. The method involves solving simultaneously for the complexation reactions (which are assumed to be at equilibrium), the kinetically-controlled heterogeneous reactions, and the transport terms. The primary species (the C_j's) rather than the "total" concentrations (the Ψ_j's) are the unknowns. Following the notation of LICHTNER (1992), we can introduce the differential operator

$$\mathcal{L}(\Psi_j) = \left[\frac{\partial}{\partial t}\phi - \frac{\partial}{\partial x}\left(\phi D \frac{\partial}{\partial x}\right)\right]\Psi_j, \qquad (A1)$$

and write the governing differential equations for solutes in terms of the "total" component concentrations as

$$\mathcal{L}(\Psi_j) = R_j^{\min} \quad (j = 1, \ldots, N_c). \qquad (A2)$$

Substituting Eqn. 2 into Eqn. 3, an expression for the "total" component concentration is obtained in terms of the primary species alone. Substituting this result and Eqn. 14 into Eqn. A2 gives (STEEFEL and LASAGA, 1994)

$$\mathcal{L}\left[C_j + \sum_{i=1}^{N_x} \nu_{ij}\gamma_i^{-1} K_i^{-1} \prod_{j=1}^{N_c} (\gamma_j C_j)^{\nu_{ij}}\right] + \sum_{m=1}^{N_m} \nu_{jm} \operatorname{sgn}\left(\log\left[\frac{Q_m}{K_m}\right]\right) A_m k_m \left(\prod_{i=1}^{N_c+N_x} a_i^{p}\right)\left|\left(\frac{Q_m}{K_m}\right)^{n} - 1\right|^{n} = 0$$

$$(j = 1, \ldots, N_c), \qquad (A3)$$

where the γ_i's and γ_j's are the activity coefficients for the secondary and primary species respectively.

The integrated finite difference method is used to convert the differential operator $\mathcal{L}$ into an algebraic expression (PATANKAR, 1980; MARSILY, 1986). In the integrated finite difference formulation, a control volume is defined and the differential equations are converted to a set of algebraic equations which include a time derivative, fluxes across the boundaries of the volume, and a reaction term (Fig. 1). Using a fully implicit formulation with respect to the solute concentrations and dropping the subscripts for the individual chemical components, Eqn. 4 can be written as

$$f_{j,i} = \frac{\phi_i^n \Psi_{j,i}^{n+1} - \phi_i^n \Psi_{j,i}^n}{\Delta t} - \frac{1}{\Delta X}\left[(\phi^n D)_{j,i+1/2} \frac{\Psi_{j,i+1}^{n+1} - \Psi_{j,i}^{n+1}}{(dx)_{i+1/2}} - (\phi^n D)_{j,i-1/2} \frac{\Psi_{j,i}^{n+1} - \Psi_{j,i-1}^{n+1}}{(dx)_{i-1/2}}\right] - R_{j,i}^{n+1} = 0, \qquad (A4)$$

where $n + 1$ and n refer to the future and present time level, respectively, the subscripts i, $i + 1$, and $i - 1$ refer to nodal points, the subscripts $i + \frac{1}{2}$ and $i - \frac{1}{2}$ denote the properties averaged between the grid points i and $i + 1$ and i and $i - 1$, respectively, and j refers to the chemical component. The spacings $(dx)_{i+1/2}$, $(dx)_{i-1/2}$, and ΔX are shown in Fig. 1. Note that we use the values of the porosity from the nth or previous time step, which is justified if the porosity is changing slowly relative to the time step used. Where this is not true, the porosity and solute concentrations must be solved for simultaneously or iteration between the two is required. The finite difference equations are written in terms of the "total" concentrations, Ψ, for the sake of compactness, but as discussed above, the actual algorithm employed by 1DREACT expresses the equations directly in terms of the primary species concentrations using Eqn. 3.

Since both the "total" concentrations, Ψ, and the heterogeneous reaction term, R, are nonlinear functions of the primary species concentrations, an iterative method is required to solve Eqn. A4. The nonlinear set of algebraic equations are solved with the Newton-Raphson method. In practice, one carries out a series of nested calculations in order to complete a time step. A number of Newton iterations are normally required to obtain convergence of the nonlinear set of algebraic equations. Each Newton iteration, in turn, requires the solution of a set of simultaneous linear equations at each nodal point within the domain in order to obtain the corrections to the primary species concentrations. It is apparent from Eqn. A4 that in a one-dimensional system, the concentrations of the primary species at a nodal point i are potentially functions of all of the primary species concentrations at the i, $i + 1$, and $i - 1$ nodal points. The logarithms of the primary species concentrations are used because of the superior numerical stability of this method. In a one-dimensional problem, therefore, a single Newton iteration requires solving a set of linear equations of the form

$$\sum_{j'=1}^{N_c} \frac{\partial f_{j,i}}{\partial \ln C_{j',i}} \delta \ln C_{j',i} + \sum_{j'=1}^{N_c} \frac{\partial f_{j,i}}{\partial \ln C_{j',i+1}} \delta \ln C_{j',i+1} + \sum_{j'=1}^{N_c} \frac{\partial f_{j,i}}{\partial \ln C_{j',i-1}} \delta \ln C_{j',i-1} = -f_{j,i}, \qquad (A5)$$

where the derivatives $\partial f_{j,i}/\partial \ln C_{j'}$, form the elements of the Jacobian matrix. Once the entire vector of concentration corrections (the $\delta \ln C_{j',i}$'s) are obtained by solving Eqn. A5 over the entire spatial domain, the concentrations are updated according to

$$\ln C_{j',i}^{k+1} = \ln C_{j',i}^{k} + \delta \ln C_{j',i}, \qquad (A6)$$

where the superscript k refers here to the iteration level. This procedure is repeated until convergence is obtained. Since Eqn. A5 has a block tridiagonal form in a one-dimensional problem, it is solved efficiently with the block tridiagonal solver developed by HINDMARSH (1977).